

APOLLO

GUIDANCE, NAVIGATION AND CONTROL

Approved: A. L. Kosmala Date: 3 Jan 69
A. L. KOSMALA, DIRECTOR, SUPPORT PROGRAM DEVEL.
APOLLO GUIDANCE AND NAVIGATION PROGRAM

Approved: Fred H. Martin Date: 1/3/69
F. H. MARTIN, COLOSSUS PROJECT MANAGER
APOLLO GUIDANCE AND NAVIGATION PROGRAM

Approved: R. H. Battin Date: 3 Jan 69
R. H. BATTIN, DIRECTOR, MISSION DEVELOPMENT
APOLLO GUIDANCE AND NAVIGATION PROGRAM

Approved: D. G. Hoag Date: 3 Jan 69
D. G. HOAG, DIRECTOR
APOLLO GUIDANCE AND NAVIGATION PROGRAM

Approved: Ralph A. Ragan Date: 3 Jan 69
R. R. RAGAN, DEPUTY DIRECTOR
INSTRUMENTATION LABORATORY

R-577

GUIDANCE SYSTEM OPERATIONS PLAN
FOR MANNED CM EARTH ORBITAL AND
LUNAR MISSIONS USING
PROGRAM COLOSSUS I (REV. 237)
AND PROGRAM COLOSSUS IA (REV. 249)

SECTION 6 CONTROL DATA
(Rev. 1)

DECEMBER 1968

**MIT INSTRUMENTATION
LABORATORY**
CAMBRIDGE 39, MASSACHUSETTS

ACKNOWLEDGEMENT

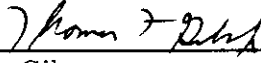
This report was prepared under DSR Project 55-23870, sponsored by the Manned Spacecraft Center of the National Aeronautics and Space Administration through Contract NAS 9-4065 with the Instrumentation Laboratory, Massachusetts Institute of Technology, Cambridge, Mass.

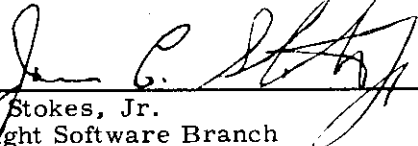
R-577

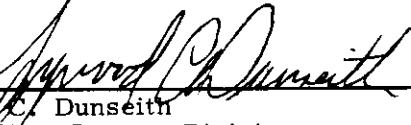
GUIDANCE SYSTEM OPERATIONS PLAN
FOR MANNED CM EARTH ORBITAL OR
LUNAR MISSIONS USING
PROGRAM COLOSSUS

SECTION 6 CONTROL DATA

Signatures appearing on this page designate approval of this document by NASA/MSC.

Approved:  Date: 1-3-68
Thomas F. Gibson
Asst. Chief, Flight Software Branch
Manned Spacecraft Center, NASA

Approved:  Date: 7/3/68
James C. Stokes, Jr.
Chief, Flight Software Branch
Manned Spacecraft Center, NASA

Approved:  Date: 9/9/68
Lynwood C. Dunseith
Chief, Flight Support Division
Manned Spacecraft Center, NASA

Date: December 1968

REVISION INDEX COVER SHEET
GUIDANCE SYSTEM OPERATIONS PLAN

GSOP # R-577 Title: For Manned CM Earth Orbital and Lunar Missions
Using Program Colossus 1 (Rev 237)

Section #6 Title: Control Data (Rev.1)

This document has been revised from the previous issue of June 1968 by the following Program Change Notifications (PCN's) which have been implemented in the COLOSSUS digital simulator with NASA/MSC approval:

Date	Rev.	Remove Pages	Add Pages	PCN Ref
Dec. 1968	1	Title page page ii page iii	Title page (Rev 1) page ii (Rev 1) page iii (Rev 1) 6-27a, 6-32a, 6-35a, 6-51a, 6-37 6-13a, 6-14a, 6-15a, 6-25a, 6-43a, 6-46a 6-57	624* 629*

* Indicates an MIT Program Change Notice (PCN)

Because the baseline data documented in this section is historical in nature, original pages have not been altered, but additional pages have been added to reflect the incorporation of new data into the simulators. Page number suffixes have been used to implement this scheme. As an example, page 6-13a was added to reflect changes to the original page 6-13. In addition, implementation dates accompany all new data.

FOREWORD

The Guidance System Operation Plan (GSOP) for Program COLOSSUS is published in six sections as separate volumes (sections) as listed below:

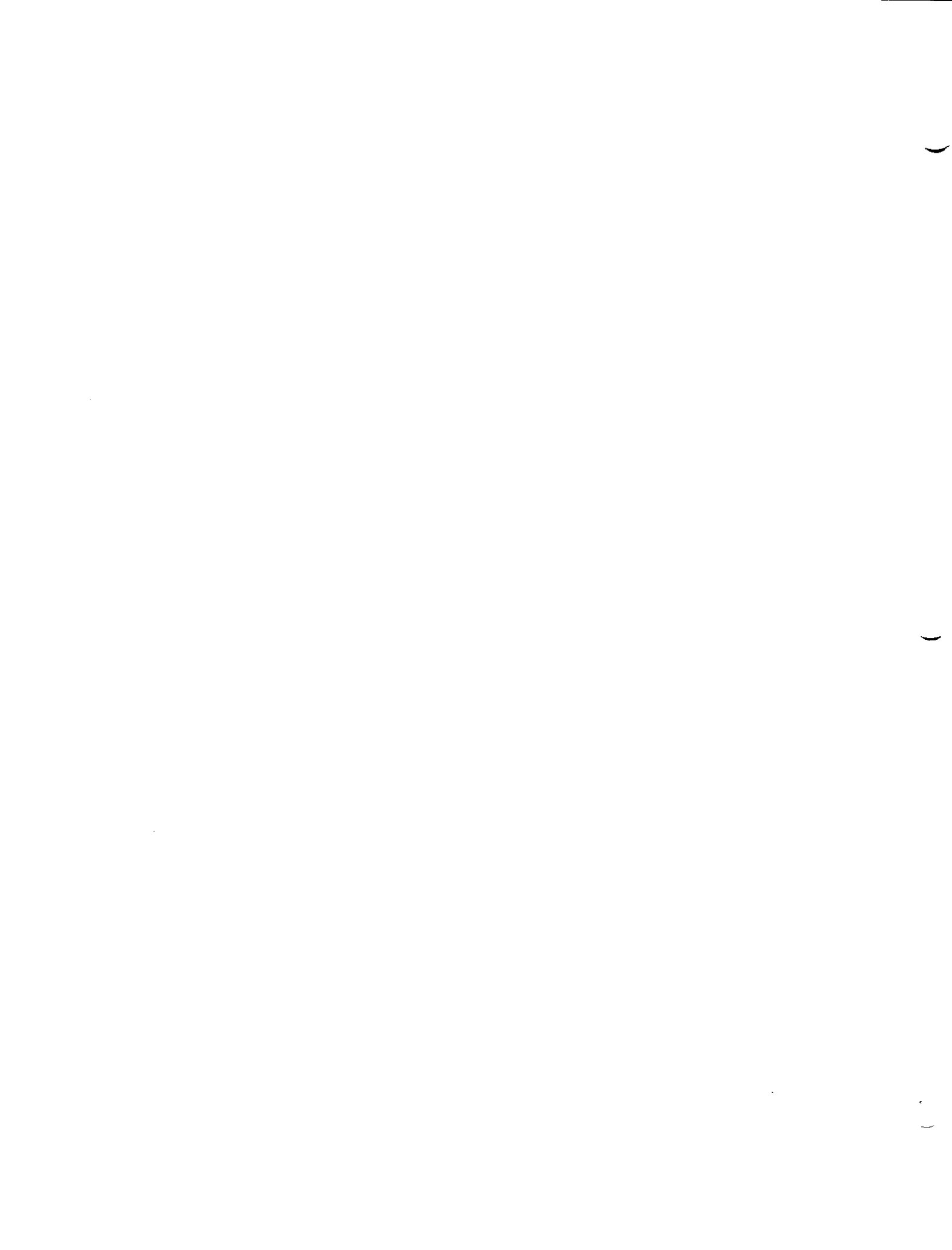
Section 1	Prelaunch
Section 2	Data Links
Section 3	Digital Autopilots
Section 4	Operational Modes
Section 5	Guidance Equations
Section 6	Control Data

This volume (Section 6) is published as a control document governing the data used in the digital and hybrid simulators in support of the verification of the AGC program COLOSSUS. The data presented herein represent the most current data available at the time the simulators underwent configuration control (17 May 68). Revision to this document requires NASA approval.

Data represented in the Digital Simulation were gathered together by Sidney S. David who prepared the major portion of the CSM section. Robert D. Wadsworth also contributed to this section. The Saturn and Prelaunch sections were prepared by Lance W. Drane. Frederick K. Glick presented the VHF Range System data. Leonard W. Silver prepared the Entry section.

The several sections corresponding to the Hybrid Simulation were presented by George J. Kossuth.

Editing and copy preparation were supervised by Joseph P. Glendenning.



6. CONTROL DATA

6.1 Introduction and Description of Simulators

6.1.1 Introduction

To formulate, code, and verify flight computer programs for an Apollo mission requires accurate, timely information regarding the mission and spacecraft characteristics. In this section (6) the data which were used in the MIT digital and hybrid simulations for the verification of the program COLOSSUS (Manned Block II Apollo Lunar Mission) are summarized. Brief discussions of the most significant mathematical models are included as well as the numerical data. The data are arranged as follows:

- Section 6.2 Digital Simulator Prelaunch Environment Data, describing the gravity and swaying booster simulation used to verify the prelaunch operations.
- Section 6.3 Digital Simulator Launch Vehicle Data, describing the key booster parameters used in the simulation from lift-off until separation of the CSM.
- Section 6.4 Digital Simulator CSM and LM Spacecraft Data, including reference positions and dimensions, mass properties, propulsion data, and dynamic models for structural bending and propellant slosh.
- Section 6.5 Digital Simulator CM Reentry Spacecraft Data, including reference positions and dimensions, mass properties, propulsion data, and reentry aerodynamics.
- Section 6.6 Digital Simulation VHF Range System, including range limitation and scale factor.
- Section 6.7 Digital Simulator Coordinate Systems and Natural Environment Data, describing models used which influence the spacecraft trajectory.
- Section 6.8 Hybrid Simulator Prelaunch Environment Data.
- Section 6.9 Hybrid Simulator Launch Vehicle Data.
- Section 6.10 Hybrid Simulator CSM and LM Spacecraft Data, including vehicle dimensions, mass properties, and dynamic models for structural bending and propellant slosh.
- Section 6.11 Hybrid Simulator CM and Reentry Spacecraft Data, including vehicle dimensions, mass properties and reentry aerodynamics.
- Section 6.12 Hybrid Simulator VHF Range System, describing the data and the interface with the AGC.

Section 6.13 Hybrid Simulator Coordinate Systems and Natural Environment Data, describing models used which influence the spacecraft trajectory.

Section 6.14 References, listing the basic source documents from which the control data and models were derived.

In Section 6.2 through 6.13 a number in the right-hand column opposite a data entry is the number of the source document as given in the Reference Section 6.14.

6.1.2 The Digital Simulator

The MIT Apollo Digital Simulator is a complex, highly flexible tool used to support design, development, and verification of onboard Apollo Guidance Computer programs. The Simulator is entirely digital - no flight hardware of any sort is incorporated in the simulation, and elements of the Simulator are represented by programs on a general purpose digital computer. The Simulator exists in the purely abstract form of a number of computer programs. Its usefulness is closely tied to the precision with which its programs represent the detailed functioning of the real hardware and flight environment. Considerable care was taken to ensure that the simulated AGC and the real AGC function identically, and that all aspects of the Apollo hardware and flight environment that interact significantly with the AGC are simulated.

6.1.3 The Hybrid Simulation

The Apollo Hybrid Simulator is a real-time simulation of the vehicle and any environment the AGC or flight crew would experience. Flight hardware such as a real CDU and real DSKY interface with a real AGC with its fixed memory replaced by a core rope simulator. The cockpit mock-up provides discretized for the AGC and man-in-the-loop capability so that procedures and mission programs can be verified. Rapid debugging is possible as AGC registers can be monitored or fixed memory changed easily, and environment and down-link data can be compared using the offline edit. Because vehicle dynamics can be simulated on analog computers and the vehicle's environment and trajectory can be computed on the digital computer, a sophisticated simulator is available to the user for real-time studies.

6.2 Digital Simulator Prelaunch Environment Data

6.2.1 To simulate a prelaunch environment, the position, velocity, gravity and time integral of gravity at the spacecraft navigation base are computed as analytic functions of time, and not by the numerical integration method used in the flight mode.

The gravitational acceleration includes perturbations due to earth oblateness, and sun and moon attractions. The centripetal acceleration due to earth rotation is then added to the gravitational acceleration vector.

Earth rotation rate expressed in the reference coordinate system	WE	0.0 0.0 72921.2×10^{-9}	rad/sec rad/sec rad/sec	2.1
North latitude of Launch Pad 39A	LAT	28.53186	deg	2.2
East longitude of Launch Pad 39A	LONG	279.43507	deg	2.2
Altitude of the spacecraft navigation base above the reference ellipsoid	ALT	96.83	m	2.3
Spacecraft +Z axis measured counterclockwise from east	AZIMUTH	180	deg	2.3

6.2.2 Superimposed on the deterministic model of gravity and earth rotation is a stochastic model for the launch vehicle swaying in the wind on the launch pad. The swaying motion is assumed to have no preferred direction, so it is modelled by two independent random processes in the two horizontal directions. The swaying booster is modelled as a damped second-order oscillator so that the displacement, r , is related to the normalized force, f , by the differential equation

$$\ddot{r} + 2 a w \dot{r} + w^2 r = f$$

Damping ratio of the vehicle for swaying motion		0.1	n/a	2.4
Natural frequency of the launch vehicle in sway		2.70	rad/sec	2.5

The wind force, f , on the side of the launch vehicle is modelled as an exponentially correlated Gaussian process. It is governed by the differential equation

$$\dot{f} + f/T = W$$

where W is a piecewise constant random forcing function whose amplitude distribution is Gaussian.

The correlation time of the wind force	T	10	sec	2.4
--	---	----	-----	-----

6.3 Digital Simulator Launch Vehicle (AS-503) Data

6.3.1 Major Events During Saturn Trajectory 3.1

The following sequence is a chronological ordering of the simulated events for a Saturn V mission. Time is always in seconds from lift-off.

Guidance reference release (ST124 platform)	GRR	-16.7	sec
SIC lift-off	LIFTOFF	0.0	sec
Lift-off signal	TBASE1	0.3	sec
Attitude hold constant for staging	ATTHOLD	153.0	sec
SIC outboard engines turned off	OUTOFF	158.754	sec
SII 90% Thrust	SII IG	164.994	sec
Launch escape tower jettisoned	LES	195.564	sec
Initiate IGM calculations	STARTIGM	201.0	sec
SII mixture ratio change	SIIMR47	432.0	sec
SII/SIVB separation	SEP	538.285	sec
SIVB 90% Thrust	SIVBLO	544.410	sec
Approximate time of SIVB cut-off	APPCO	661.439	sec

6.3.2 Pre-Iterative Guidance Mode Pitch Polynomials 3.5

Open loop steering commands are generated during SIC flight through the atmosphere by a fourth order polynomial function of time from lift-off.

$$\text{PITCH} = \sum_{J=0}^4 F_J T^J \quad \text{deg}$$

	Time period 0.0 < t < 13.0	sec
PITCH =	0	
	Time Period 13.0 < t < 35.0	sec
F ₀	3.19840	deg
F ₁	-0.544236	deg/sec
F ₂	0.0351605	deg/sec ²
F ₃	-0.00116379	deg/sec ³
F ₄	0.0000113886	deg/sec ⁴
	Time Period 35.0 < t < 80.0	sec
F ₀	-10.9607	deg
F ₁	0.946620	deg/sec
F ₂	-0.0294206	deg/sec ²
F ₃	0.000207717	deg/sec ³
F ₄	-0.000000439036	deg/sec ⁴
	Time Period 80.0 < t < 115.0	sec
F ₀	78.7826	deg
F ₁	-2.83749	deg/sec
F ₂	0.0289710	deg/sec ²
F ₃	-0.000178363	deg/sec ³
F ₄	0.000000463029	deg/sec ⁴

Time Period 115.0 < t < 153.0 sec

F ₀	69.9191	deg
F ₁	-2.007490	deg/sec
F ₂	0.0105367	deg/sec ²
F ₃	-0.0000233163	deg/sec ³
F ₄	0.0000000136702	deg/sec ⁴

6.3.3 Parking Orbit Insertion Guidance 3.1

Steering commands during SIVB burn for parking orbit insertion are generated by solving the closed loop Iterative Guidance Mode equations.

The IGM steering terminal conditions are:

Launch azimuth measured clock- wise from north	72.0	deg
Terminal geocentric radius magnitude	6563365.1	m
Terminal inertial velocity magnitude	7749.955	m/sec
Terminal flight path angle	0.0	deg
Inclination of orbit	32.55754	deg
Descending node of orbit	123.1935	deg

6.3.4 Thrust Simulation 3.3

6.3.4.1 To simulate the time thrust of the five F1 engines of the SIC stage, thrust is simulated as a step function of time from lift-off. This reflects the actual change in thrust of the engines and does not include forces caused by atmospheric drag.

Time	Thrust	
0.0	33 938 250	newtons
2.5	33 971 990	newtons
7.5	34 034 200	newtons
12.5	34 132 540	newtons
17.5	34 270 180	newtons
22.5	34 449 660	newtons
27.5	34 672 080	newtons
32.5	34 939 320	newtons
37.5	35 248 680	newtons
42.5	35 596 560	newtons
47.5	35 976 510	newtons
52.5	36 377 720	newtons
57.5	36 789 440	newtons
62.5	37 200 670	newtons
67.5	37 599 950	newtons
72.5	37 989 150	newtons
77.5	38 357 830	newtons
83.0	38 561 320	newtons
85.0	38 688 970	newtons
90.0	38 976 740	newtons
95.0	39 212 910	newtons
100.0	39 403 610	newtons
105.0	39 559 480	newtons
110.0	39 692 710	newtons
115.0	39 812 460	newtons
120.0	39 926 380	newtons
125.0	40 039 970	newtons

Time	Thrust	
130.0	40 158 150	newtons
135.0	40 285 400	newtons
140.0	40 426 160	newtons
145.0	40 585 170	newtons
150.0	40 768 200	newtons
154.524	32 768 450	newtons

6.3.4.2 Thrust of the SII stage is simulated as constant.

Average thrust of the five J2 engines of the SII stage	5115450	newtons
--	---------	---------

Average thrust after fuel mixture ratio shift	4225810	newtons
---	---------	---------

6.3.4.3 Thrust of the SIVB stage is simulated as constant.

Average thrust of the J2 engine of the SIVB stage first burn first fuel mixture ratio	889652	newtons
---	--------	---------

Average thrust of the J2 engine of the SIVB stage first burn second fuel mixture ratio	911885.4	newtons
--	----------	---------

6.3.5 Mass History and Mass Decrement Rates

3.3

6.3.5.1 The following data describe the mass history of the Saturn V trajectory.

Total Mass of SIC and SII and SIVB and Apollo Configurations with frost, LES, and all other masses at lift off.	2903620	kg
---	---------	----

Total Mass of SII and SIVB, Apollo Configuration, LES, ullage cases, and all other masses at SII ignition.	661450	kg
--	--------	----

Total Mass of SIVB and Apollo Configuration at SIVB ignition.	164855	kg
---	--------	----

6.3.5.2 The following data describe the mass decrement rates of the Saturn V trajectory.

Average mass decrement rate during the SIC burn caused by fuel consumed, by frost burned off, and by all other changes in mass not submitted as a specific mass decrement	13185	kg/sec
Average mass decrement rate during the SII burn first mixture ratio.	1265	kg/sec
Average mass decrement rate during the SII burn second mixture ratio.	1010	kg/sec
Average mass decrement rate during the first SIVB burn first mixture ratio.	226	kg/sec

6.3.6 Flight Control Computer control loop gains during SIC, SII, and SIVB burns.

3.4

TIME	ERROR GAIN A_0 rad/rad		RATE GAINS A_1 rad/(rad/sec)	
	ROLL	PITCH & YAW	ROLL	PITCH & YAW
SIC Lift-off	0.245	0.82	0.15	0.657
SIC Lift-off + 100	0.245	0.45	0.15	0.438
SIC Lift-off + 120	0.245	0.15	0.15	0.2
SII Ignition	0.25	1.12	0.2	1.89
SII Ignition + 60	0.25	0.65	0.2	1.10
SII Ignition + 190	0.25	0.44	0.2	0.74
SIVB Ignition	1.0	0.809	5.0	0.97
SIVB Cut-off	1.0	1.0	5.0	5.0

6.4 Digital Simulator CSM (CSM-103) and LM (LM-3) Spacecraft Data

6.4.1 CSM Reference Positions and Dimensions

The following reference positions and dimensions are expressed in the Apollo coordinate system in the order X component, Y component, Z component unless otherwise noted.

6.4.1.1	CM Navigation Base	NB	1055.715	in.	4.1
	Position		0.0	in	
	Intersection of the three accelerometer input axes.		40.914	in.	

6.4.1.2	SPS Gimbal Ring	SP	833.2	in.	4.2
	Position		0.0	in.	
	Intersection of the two gimbal ring axes.		0.0	in.	

6.4.1.3 RCS Quad Location and Jet Orientation 4.2

Each of the 4 RCS jet quads are located at the same point on the X axis. The quads are 90 degrees apart in the Y-Z plane. They are offset from alignment with the Y and Z axes by a negative rotation about the +X axis in accordance with the right-hand rule. The engine nozzles are positioned (canted) such that the exhaust gases are directed away from the spacecraft surface. The distance from the X axis to the RCS jet centerline intersection has been averaged and is modelled as a constant for each quad. See Fig. 2.9 of Reference 4.2.

X axis location of all RCS Quads	RCRX	958.97	in.
Average distance from X axis to RCS jet centerline intersection	RCRAD	82.68	in.
RCS quad offset from Y and Z axes	OFFSET	7.25	deg
Nozzle cant angle	CANT	10.0	deg

6.4.2 LM/CSM Coordinate Transformation

4.3

Prior to the simulated mission, when the LM mass is selected, its center of gravity and inertia are computed in the LM coordinate system (Section 6.4.4). These parameters are subsequently transformed into the Apollo coordinate system. The relation between the Apollo and LM vehicle coordinates is given below in terms of the displacement of the LM origin in the Apollo coordinate system and a transformation matrix. The transformations are as follows:

$$\underline{CG}_{APOLLO} = \overset{*}{TEMP} \overset{*}{CG}_{LM} + \underline{DISP}$$

$$\overset{*}{INERTIA}_{APOLLO} = \overset{*}{TEMP} \overset{*}{INERTIA}_{LM} \overset{*}{TEMP}^T$$

Position of LM coordinate origin in Apollo coordinates	X	DISP	1422.75	in.
	Y		0.0	in.
	Z		0.0	in.
Transformation matrix from LM to Apollo Coordinates		TEMP	-1.0	nd
			0.0	
			0.0	
			0.0	
			0.5	
			0.86603	
			0.0	
			0.86603	
			-0.5	

6.4.3 CSM Mass Properties

The CSM mass properties are presented for the vehicle components and several propellant loadings. The center of gravity is expressed in the Apollo coordinate system. The inertia is about the center of gravity of each item and is given with respect to the Apollo coordinate directions. Both the diagonal and off-diagonal elements of the inertia tensor are used as positive elements. Hence the numerical values of the off-diagonal elements reported below have signs opposite to those given in the referenced documents.

Prior to the simulation, the masses, center of gravities and inertias of all vehicle components (including propellants and the docked LM if desired) are appropriately combined. During the simulated mission, the vehicle mass is decremented by propellant usage, and vehicle center of gravity and inertia are recalculated.

6.4.3.1 Empty Service Module Including Total

Service Module RCS Propellant and SPS System Residuals 4.3

Mass		MSM	10800	lb
Center of Gravity	X	CGSM	918.0	in.
	Y		-6.0	in.
	Z		10.3	in.
Inertia	I _{XX}	ISM	7337.0	slug ft ²
	I _{YY}		12222.0	slug ft ²
	I _{ZZ}		11745.0	slug ft ²
	I _{XY}		96.7	slug ft ²
	I _{XZ}		-321.3	slug ft ²
	I _{YZ}		186.4	slug ft ²

6.4.3.2 Spacecraft Lunar Module Adapter Attach Ring

4.3

Mass		MSLAR	91.0	lb
Center of Gravity	X	CGSLAR	837.1	in.
	Y		-0.3	in.
	Z		1.9	in.
Inertia	I _{XX}	ISLAR	113.0	slug ft ²
	I _{YY}		58.0	slug ft ²
	I _{ZZ}		55.0	slug ft ²
	I _{XY}		0.0	slug ft ²
	I _{XZ}		0.0	slug ft ²
	I _{YZ}		0.0	slug ft ²

Prior to the simulation, the masses, center of gravities and inertias of all vehicle components (including propellants and the docked LM if desired) are appropriately combined. During the simulated mission, the vehicle mass is decremented by propellant usage, and vehicle center of gravity and inertia are recalculated.

6.4.3.1 Empty Service Module Including Total

Service Module RCS Propellant and SPS System Residuals 4.3

Mass		MSM	10675	lb	9/30/68
Center of Gravity	X	CGSM	918.7	in.	9/30/68
	Y		-5.7	in.	9/30/68
	Z		11.2	in.	9/30/68
Inertia	I_{XX}	ISM	7340.0	slug ft ²	9/30/68
	I_{YY}		12250.0	slug ft ²	9/30/68
	I_{ZZ}		11725.0	slug ft ²	9/30/68
	I_{XY}		90.0	slug ft ²	9/30/68
	I_{XZ}		-430.0	slug ft ²	9/30/68
	I_{YZ}		600.0	slug ft ²	9/30/68

6.4.3.2 Spacecraft Lunar Module Adapter Attach Ring

4.3

Mass		MSLAR	91.0	lb	
Center of Gravity	X	CGSLAR	837.1	in.	
	Y		-0.3	in.	
	Z		1.9	in.	
Inertia	I_{XX}	ISLAR	113.0	slug ft ²	
	I_{YY}		58.0	slug ft ²	
	I_{ZZ}		55.0	slug ft ²	
	I_{XY}		0.0	slug ft ²	
	I_{XZ}		0.0	slug ft ²	
	I_{YZ}		0.0	slug ft ²	

6.4.3.3 Nominal Full Command Module, including CM RCS Propellants 4.3

Mass		MCM	13065.0	lb	
Center of Gravity	X	CGCM	1042.8	in.	
	Y		-0.5	in.	
	Z		5.3	in.	
Inertia	I_{XX}	ICM	6032.0	slug ft ²	
	I_{YY}		5575.0	slug ft ²	
	I_{ZZ}		5043.0	slug ft ²	
	I_{XY}		-56.4	slug ft ²	
	I_{XZ}		440.6	slug ft ²	
	I_{YZ}		-13.2	slug ft ²	

6.4.3.4 Service Module RCS Propellant Mass Properties

During the simulated mission, the RCS propellant center of gravity is modelled as a constant. The propellant inertia is found by a linear interpolation between two tabulated points; one of which corresponds to zero mass, zero inertia, and the other which corresponds to an approximate full load.

Usable Service Module RCS propellant loaded for this mission		MRCINIT	1317.2	lb	4.4
--	--	---------	--------	----	-----

RCS Propellant Loading 100%

Mass (Usable)		MRCINIT	1317.2	lb	4.4
Center of Gravity	X	CGRCS	941.8	in.	4.4
	Y		0.0	in.	
	Z		0.0	in.	
Inertia	I_{XX}	IR	1250.0	slug ft ²	4.5
	I_{YY}		750.0	slug ft ²	
	I_{ZZ}		700.0	slug ft ²	
	I_{XY}		0.0	slug ft ²	
	I_{XZ}		0.0	slug ft ²	
	I_{YZ}		0.0	slug ft ²	

6.4.3.3 Nominal Full Command Module, including CM RCS Propellants 4.3

Mass		MCM	12392.0	lb	9/30/68
Center of Gravity	X	CGCM	1042.1	in.	9/30/68
	Y		-0.2	in.	9/30/68
	Z		5.8	in.	9/30/68
Inertia	I_{XX}	ICM	5800.0	slug ft ²	9/30/68
	I_{YY}		5220.0	slug ft ²	9/30/68
	I_{ZZ}		4725.0	slug ft ²	9/30/68
	I_{XY}		-40.0	slug ft ²	9/30/68
	I_{XZ}		420.0	slug ft ²	9/30/68
	I_{YZ}		-15.0	slug ft ²	9/30/68

6.4.3.4 Service Module RCS Propellant Mass Properties

During the simulated mission, the RCS propellant center of gravity is modelled as a constant. The propellant inertia is found by a linear interpolation between two tabulated points; one of which corresponds to zero mass, zero inertia, and the other which corresponds to an approximate full load.

Usable Service Module RCS propellant loaded for this mission		MRCINIT	1317.2	lb	4.4
--	--	---------	--------	----	-----

RCS Propellant Loading 100%

Mass (Usable)		MRCINIT	1317.2	lb	4.4
Center of Gravity	X	CGRCS	941.8	in.	4.4
	Y		0.0	in.	
	Z		0.0	in.	
Inertia	I_{XX}	IR	1250.0	slug ft ²	4.5
	I_{YY}		750.0	slug ft ²	
	I_{ZZ}		700.0	slug ft ²	
	I_{XY}		0.0	slug ft ²	
	I_{XZ}		0.0	slug ft ²	
	I_{YZ}		0.0	slug ft ²	

6-14a

Revised COLOSSUS

Added GSOP #R-577 PCR # 629 Rev. 1 Date 12/68

6.4.3.5 Service Module SPS Propellant Mass Properties

The Service Module SPS Propellant mass properties are presented at three different propellant loadings for each of the four propellant tanks. Prior to the simulation, these mass properties are appropriately combined to produce two sets of mass properties at three different propellant loadings for both the combined storage tanks and the combined sump tanks. During the simulated mission, depending upon the propellant level, the propellant center of gravity is found by a linear interpolation between two calculated points; and the inertia is found by a cubic interpolation between three calculated points.

Since SPS propellant loading is mission dependent and the predicted value frequently varies prior to the mission, the capability to change this parameter within the simulation exists. It is incumbent upon the users of the simulator to keep abreast of mission planning and select the appropriate propellant loading to meet their particular objectives.

Tanked Service Module SPS propellant mass		MSPINIT	35268.0	lb	4.3
Sump tank propellant mass capacity		MSUMP	22300.0	lb	4.6
Sump tank propellant residual		MSPRESID	239.0	lb	4.3
<u>Oxidizer Storage Tank</u>					4.2
Propellant Loading No. 1					
Mass		MSO ₀	3746.84	lb	
Center of Gravity	X	RSO ₀	861.8	in.	
	Y		14.8	in.	
	Z		47.8	in.	
Inertia	I _{XX}	ISO ₀	0.0	slug ft ²	
	I _{YY}		244.6	slug ft ²	
	I _{ZZ}		244.6	slug ft ²	
	I _{XY}		0.0	slug ft ²	
	I _{XZ}		0.0	slug ft ²	
	I _{YZ}		0.0	slug ft ²	

6.4.3.5 Service Module SPS Propellant Mass Properties

The Service Module SPS Propellant mass properties are presented at three different propellant loadings for each of the four propellant tanks. Prior to the simulation, these mass properties are appropriately combined to produce two sets of mass properties at three different propellant loadings for both the combined storage tanks and the combined sump tanks. During the simulated mission, depending upon the propellant level, the propellant center of gravity is found by a linear interpolation between two calculated points; and the inertia is found by a cubic interpolation between three calculated points.

Since SPS propellant loading is mission dependent and the predicted value frequently varies prior to the mission, the capability to change this parameter within the simulation exists. It is incumbent upon the users of the simulator to keep abreast of mission planning and select the appropriate propellant loading to meet their particular objectives.

Tanked Service Module SPS propellant mass		MSPINIT	40583.0	lb	9/30/68	4.3
Sump tank propellant mass capacity		MSUMP	22300.0	lb		4.6
Sump tank propellant residual		MSPRESID	239.0	lb		4.3
<u>Oxidizer Storage Tank</u>						4.2
Propellant Loading No. 1						
Mass		MSO ₀	3746.84	lb		
Center of Gravity	X	RSO ₀	861.8	in.		
	Y		14.8	in.		
	Z		47.8	in.		
Inertia	I _{XX}	ISO ₀	0.0	slug ft ²		
	I _{YY}		244.6	slug ft ²		
	I _{ZZ}		244.6	slug ft ²		
	I _{XY}		0.0	slug ft ²		
	I _{XZ}		0.0	slug ft ²		
	I _{YZ}		0.0	slug ft ²		

Propellant Loading No. 2

Mass		MSO ₁	7579.05	lb
Center of Gravity	X	RSO ₃	885.1	in.
	Y		14.8	in.
	Z		47.8	in.
Inertia	I _{XX}	ISO ₉	0.0	slug ft ²
	I _{YY}		1362.0	slug ft ²
	I _{ZZ}		1362.0	slug ft ²
	I _{XY}		0.0	slug ft ²
	I _{XZ}		0.0	slug ft ²
	I _{YZ}		0.0	slug ft ²

Propellant Loading No. 3

Mass		MSO ₂	11084.90	lb
Center of Gravity	X	RSO ₆	906.2	in.
	Y		14.8	in.
	Z		47.8	in.
Inertia	I _{XX}	ISO ₁₈	0.0	slug ft ²
	I _{YY}		3891.1	slug ft ²
	I _{ZZ}		3891.1	slug ft ²
	I _{XY}		0.0	slug ft ²
	I _{XZ}		0.0	slug ft ²
	I _{YZ}		0.0	slug ft ²

Fuel Storage Tank

4.2

Propellant Loading No. 1

Mass		MSF ₀	2343.24	lb
Center of Gravity	X	RSF ₀	861.8	in.
	Y		-14.8	in.
	Z		-47.8	in.

Inertia	I_{XX}	ISF ₀	0.0	slug ft ²
	I_{YY}		153.0	slug ft ²
	I_{ZZ}		153.0	slug ft ²
	I_{XY}		0.0	slug ft ²
	I_{XZ}		0.0	slug ft ²
	I_{YZ}		0.0	slug ft ²

Propellant Loading No. 2

Mass		MSF ₁	4739.87	lb
Center of Gravity	X	RSF ₃	885.1	in.
	Y		-14.8	in.
	Z		-47.8	in.
Inertia	I_{XX}	ISF ₉	0.0	slug ft ²
	I_{YY}		851.8	slug ft ²
	I_{ZZ}		851.8	slug ft ²
	I_{XY}		0.0	slug ft ²
	I_{XZ}		0.0	slug ft ²
	I_{YZ}		0.0	slug ft ²

Propellant Loading No. 3

Mass		MSF ₂	6932.40	lb
Center of Gravity	X	RSF ₆	906.2	in.
	Y		-14.8	in.
	Z		-47.8	in.
Inertia	I_{XX}	RSF ₁₈	0.0	slug ft ²
	I_{YY}		2433.4	slug ft ²
	I_{ZZ}		2433.4	slug ft ²
	I_{XY}		0.0	slug ft ²
	I_{XZ}		0.0	slug ft ²
	I_{YZ}		0.0	slug ft ²

Oxidizer Sump Tank

4.2

Propellant Loading No. 1

Mass		MSO ₃	4684.25	lb
Center of Gravity	X	RSO ₉	862.1	in.
	Y		48.3	in.
	Z		6.6	in.
Inertia	I _{XX}	ISO ₂₇	0.0	slug ft ²
	I _{YY}		331.9	slug ft ²
	I _{ZZ}		331.9	slug ft ²
	I _{XY}		0.0	slug ft ²
	I _{XZ}		0.0	slug ft ²
	I _{YZ}		0.0	slug ft ²

Propellant Loading No. 2

Mass		MSO ₄	9155.85	lb
Center of Gravity	X	RSO ₁₂	883.3	in.
	Y		48.3	in.
	Z		6.6	in.
Inertia	I _{XX}	ISO ₃₆	0.0	slug ft ²
	I _{YY}		1561.2	slug ft ²
	I _{ZZ}		1561.2	slug ft ²
	I _{XY}		0.0	slug ft ²
	I _{XZ}		0.0	slug ft ²
	I _{YZ}		0.0	slug ft ²

Propellant Loading No. 3

Mass		MSO ₅	13798.30	lb
Center of Gravity	X	RSO ₁₅	905.2	in.
	Y		48.3	in.
	Z		6.6	in.

Inertia	I_{XX}	ISO ₄₅	0.0	slug ft ²
	I_{YY}		4694.6	slug ft ²
	I_{ZZ}		4694.6	slug ft ²
	I_{XY}		0.0	slug ft ²
	I_{XZ}		0.0	slug ft ²
	I_{YZ}		0.0	slug ft ²

Fuel Sump Tank

4.2

Propellant Loading No. 1

Mass		MSF ₃	2929.47	lb
Center of Gravity	X	RSF ₉	862.1	in.
	Y		-48.3	in.
	Z		-6.6	in.
Inertia	I_{XX}	ISF ₂₇	0.0	slug ft ²
	I_{YY}		207.6	slug ft ²
	I_{ZZ}		207.6	slug ft ²
	I_{XY}		0.0	slug ft ²
	I_{XZ}		0.0	slug ft ²
	I_{YZ}		0.0	slug ft ²

Propellant Loading No. 2

Mass		MSF ₄	5725.97	lb
Center of Gravity	X	RSF ₁₂	883.3	in.
	Y		-48.3	in.
	Z		-6.6	in.
Inertia	I_{XX}	ISF ₃₆	0.0	slug ft ²
	I_{YY}		976.3	slug ft ²
	I_{ZZ}		976.3	slug ft ²
	I_{XY}		0.0	slug ft ²
	I_{XZ}		0.0	slug ft ²
	I_{YZ}		0.0	slug ft ²

Propellant Loading No. 3

Mass		MSF ₅	8629.30	lb
Center of Gravity	X	RSF ₁₅	905.2	in.
	Y		-48.3	in.
	Z		-6.6	in.
Inertial	I _{XX}	ISF ₄₅	0.0	slug ft ²
	I _{YY}		2935.9	slug ft ²
	I _{ZZ}		2935.9	slug ft ²
	I _{XY}		0.0	slug ft ²
	I _{XZ}		0.0	slug ft ²
	I _{YZ}		0.0	slug ft ²

6.4.4 LM Mass Properties

When the CSM is the controlling vehicle, there exists within the simulator the capability of simulating a constant-mass docked LM vehicle in either the ascent-descent or the ascent-only configuration. The LM mass properties are presented at three propellant loadings for both of these configurations. At each propellant loading the initial tanked RCS propellant mass is included. The LM is unmanned. The masses of the LM propellants are assumed constant and located at the CSM end of the tanks. The inertia of each propellant loading is calculated assuming that the liquid propellant is composed of a rigid mass and a sloshing mass and has no moment of inertia about its own axis (the liquid is irrotational, see reference 4.8). As is described in section 6.4.2, the center of gravity of the vehicle at each propellant loading has been transformed to and is expressed in the Apollo coordinate system. The inertia is about this center of gravity and is given with respect to the Apollo coordinate direction. Both the diagonal and off-diagonal elements of the inertia tensor are used as positive elements. Hence, the numerical values of the off-diagonal elements reported below have signs opposite to those given in the referenced documents.

Prior to the simulation, when the LM mass is selected, the center of gravity and inertia are calculated. This is achieved by a parabolic interpolation between the tabulated entries listed below for the appropriate configuration.

Since APS and DPS propellant loadings are mission dependent and their predicted values frequently vary prior to the mission, the capability to change these parameters within the simulator exists. It is incumbent upon the users of the simulator to keep abreast of mission planning and select the appropriate propellant loadings to meet their particular objectives.

6.4.4.1 Ascent-Descent Configuration

4.7

The landing gear is deployed.

Descent Stage

DPS propellant loading 100% of usable

Ascent Stage

APS propellant loading 100% of usable

Mass		32637.0	lb
Center of Gravity	X	1235.7	in.
	Y	0.02	in.
	Z	0.71	in.
Inertia	I_{XX}	21531.0	slug ft ²
	I_{YY}	23764.0	slug ft ²
	I_{ZZ}	24221.0	slug ft ²
	I_{XY}	387.0	slug ft ²
	I_{XZ}	-247.0	slug ft ²
	I_{YZ}	-395.0	slug ft ²

Descent Stage

DPS propellant loading 50% of usable

Ascent Stage

APS propellant loading 100% of usable

Mass		23869.0	lb
Center of Gravity	X	1225.3	in.
	Y	0.07	in.
	Z	0.93	in.

Inertia	I_{XX}	15862.0	slug ft ²
	I_{YY}	18433.0	slug ft ²
	I_{ZZ}	18216.0	slug ft ²
	I_{XY}	388.0	slug ft ²
	I_{XZ}	-314.0	slug ft ²
	I_{YZ}	-981.0	slug ft ²

Descent Stage

DPS propellant loading 0% of usable

Ascent Stage

APS propellant loading 100% of usable

Mass 15102.0 lb

Center of Gravity X 1205.7 in.
 Y 0.18 in.
 Z 1.40 in.

Inertia	I_{XX}	10508.0	slug ft ²
	I_{YY}	13450.0	slug ft ²
	I_{ZZ}	12641.0	slug ft ²
	I_{XY}	384.0	slug ft ²
	I_{XZ}	-397.0	slug ft ²
	I_{YZ}	-1496.0	slug ft ²

6.4.4.2 Ascent-Only Configuration

4.7

Ascent Stage

APS Propellant loading 100% of usable

Mass 10610.0 lb

Center of Gravity X 1178.2 in.
 Y 0.62 in.
 Z -0.56 in.

Inertia	I_{XX}	6645.0	slug ft ²
	I_{YY}	5391.0	slug ft ²
	I_{ZZ}	3970.0	slug ft ²
	I_{XY}	154.0	slug ft ²
	I_{XZ}	-27.0	slug ft ²
	I_{YZ}	-1170.0	slug ft ²

Ascent Stage

APS propellant loading 50% of usable

Mass		8079.0	lb
Center of Gravity	X	1173.1	in.
	Y	0.82	in.
	Z	-0.79	in.

Inertia	I_{XX}	4920.0	slug ft ²
	I_{YY}	3897.0	slug ft ²
	I_{ZZ}	3338.0	slug ft ²
	I_{XY}	147.0	slug ft ²
	I_{XZ}	-19.0	slug ft ²
	I_{YZ}	-423.0	slug ft ²

Ascent Stage

APS propellant loading 0% of usable

Mass		5548.0	lb
Center of Gravity	X	1163.4	in.
	Y	1.26	in.
	Z	-1.10	in.

Inertia	I_{XX}	3189.0	slug ft ²
	I_{YY}	2232.0	slug ft ²
	I_{ZZ}	2538.0	slug ft ²
	I_{XY}	131.0	slug ft ²
	I_{XZ}	-8.0	slug ft ²
	I_{YZ}	325.0	slug ft ²

6.4.5 SM Reaction Control System Performance

4.2

The SM Reaction Control System contains 16 thrust chambers in four separate and independent quads of four thrust chambers each. The individual RCS thruster is modelled as a constant-thrust motor.

6.4.5.1 The buildup and tailoff of thrust are modelled by instantaneous changes in thrust, shifted in time from electrical command. The shift is different for the application and removal of thrust. The amount of the shift is calculated to give a transient impulse typical of a real thruster.

Constant RCS thrust	RCTHRUST	99.8	lb
Step delay in RCS thrust application from receipt of electrical command	RCONDEL	0.015	sec
Step delay in RCS thrust removal from removal of electrical command	RCOFFDEL	0.0105	sec
Minimum allowable RCS electrical pulse width	TMINPULS	0.014	sec

6.4.5.2 The propellant usage of each RCS thruster is modelled by a constant mass flow rate when the jet is fired, plus a propellant penalty for each jet firing.

Constant RCS propellant flow rate	RCMFLO	0.361	lb/sec
Propellant penalty per jet firing	NFIRTOKG	0.0033	lb

6.4.6 Service Propulsion System

6.4.6.1 Steady and Transient Performance

The SPS engine is modelled as a constant-thrust constant-flow-rate motor. The buildup and tailoff of thrust are modelled by instantaneous changes in thrust, shifted in time from electrical command. The shift is different for the application and removal of thrust. The amount of the shift is calculated to give a transient impulse typical of the real engine.

To simulate SPS burn durations between 400 milliseconds and one second, nominal SPS minimum impulse test data are used to calculate total impulse (see reference 4.2). For burn durations of less than 400 milliseconds, a zero-impulse model is employed.

Constant SPS thrust	SPTHRUST	20500.0	lb	4.9
Step delay in SPS thrust application from receipt of electrical command	SPONDEL	0.52	sec	4.9
Step delay in SPS thrust removal from removal of electrical command	SPOFFDEL	0.49	sec	4.9
Minimum SPS pulse duration for non-zero impulse	TSPMINPL	0.40	sec	4.2
Actual time from removal of electrical command to 1.0 percent thrust (during which thrust vector control should be maintained)	SPOFFTRANS	2.2	sec	4.9
Constant SPS propellant flow rate	SPMFLO	63.8	lb/sec	4.6
6.4.6.2 Actuator Dynamics				4.2

The SPS engine is mounted on a gimbal system which permits angular motion in pitch and yaw. Engine angular position is controlled by closed-loop servomechanisms in both axes. The servo loops include an amplifier (modelled as a constant gain, no lags), a clutch (modelled as a constant gain - torquer/current ratio, no lags), position feedback and rate feedback. For small signal inputs, the operation of the servos is linear. The total torque applied to the SPS engine includes clutch torque, angular velocity dependent torques caused by damping within the actuator and exhaust jet damping, angular position dependent torques caused by hose stiffness and snubber spring stiffness (if the angular deflection exceeds the position limit), and reaction torques caused by the acceleration of the vehicle. The angular acceleration of the engine is the ratio of total torque to total inertia and is integrated twice to obtain angular deflection. Total inertia includes both engine inertia and actuator inertia.

To simulate SPS burn durations between 400 milliseconds and one second, nominal SPS minimum impulse test data are used to calculate total impulse (see reference 4.2). For burn durations of less than 400 milliseconds, a zero-impulse model is employed.

Constant SPS thrust	SPTHURST	21118.0	lb	9/30/68	4.9
Step delay in SPS thrust application from receipt of electrical command	SPONDEL	0.52	sec		4.9
Step delay in SPS thrust removal from removal of electrical command	SPOFFDEL	0.49	sec		4.9
Minimum SPS pulse duration for non-zero impulse	TSPMINPL	0.40	sec		4.2
Actual time from removal of electrical command to 1.0 percent thrust (during which thrust vector control should be maintained)	SPOFFTRANS	2.2	sec		4.9
Constant SPS propellant flow rate	SPMFLO	67.2	lb/sec	9/30/68	4.6

6.4.6.2 Actuator Dynamics 4.2

The SPS engine is mounted on a gimbal system which permits angular motion in pitch and yaw. Engine angular position is controlled by closed-loop servomechanisms in both axes. The servo loops include an amplifier (modelled as a constant gain, no lags), a clutch (modelled as a constant gain - torquer/current ratio, no lags), position feedback and rate feedback. For small signal inputs, the operation of the servos is linear. The total torque applied to the SPS engine includes clutch torque, angular velocity dependent torques caused by damping within the actuator and exhaust jet damping, angular position dependent torques caused by hose stiffness and snubber spring stiffness (if the angular deflection exceeds the position limit), and reaction torques caused by the acceleration of the vehicle. The angular acceleration of the engine is the ratio of total torque to total inertia and is integrated twice to obtain angular deflection. Total inertia includes both engine inertia and actuator inertia.

Revised COLOSSUS

Added GSOP #R-577 PCR # 629 Rev. 1 Date 12/68

Servo amplifier gain	KS	20.0	amp/rad
Actuator clutch gain	KT	3480.0	ft lb/amp
Position feedback gain	KD	1.0	nd
Rate feedback gain	KG	0.089	sec
Actuator damping (reflected to engine)	CAD	1600.0	ft lb sec per rad
Engine exhaust jet damping	CJD	171.0	ft lb sec per rad
Hose stiffness	KH	285.0	ft lb/rad
Snubber spring stiffness	KL	29400.0	ft lb/deg
Engine inertia about gimbal axis (average of pitch and yaw - wet)	IR	240.5	slug ft ²
Actuator inertia (reflected to engine)	IA	68.0	slug ft ²
Engine mass	ME	25.4	slugs
Engine moment arm (distance from center of gravity to gimbal axis)	LE	0.271	ft

6.4.6.3 Actuator and CDU Limit Data

4.2

The operation of the SPS engine gimbal servomechanisms is non-linear in several respects. The commanded angular position is limited within the digital-to-analog converter which provides the signal. (The D/A converters are located within the optics CDUs.) The torque applied by the actuators is limited by the maximum torque which the clutches can transmit. Angular rate is limited by the actuator motor speed and is modelled as a fixed gimbal rate limit. The engine angular position is limited by snubbers (stiff springs) beyond a limited range of motion. Angular position is measured with respect to the engine mount. The mount is offset in angular position with respect to vehicle axes in both

pitch and yaw. Therefore, the angle between the thrust vector direction and the vehicle axis will be the sum of the engine angular position and the engine mount angular offset. Angular positions are measured as positive rotations of the engine about the vehicle Y and Z axes (e. g. a positive engine angular position in pitch will result in a negative pitch acceleration of the vehicle).

Optics D/A limit (optics error counter)	LMP	384	pulses
Scale factor: pulse count to gimbal angle command	RPP	1.52	arc min per pulse
Pulse train rate	PPS	3200	pulses per sec
Clutch torque limit	LMT	1300	ft lb
Gimbal rate limit	LMR	0.15	rad/sec
Gimbal position limit	LMG	4.5	deg
Engine gimbal mounting offset-pitch	YBIAS	-2.15	deg
Engine gimbal mounting offset-yaw	ZBIAS	0.95	deg

6.4.7 CSM/LM Bending

It is necessary to simulate the structural deflections of the spacecraft caused by external loadings or contact forces such as main propulsion system thrust, RCS thrust, and fuel slosh. These structural deflections influence the spacecraft control systems by deflecting the navigation base. The bending deflection of the spacecraft can be expanded in terms of an infinite number of orthogonal eigenfunctions or modes and their associated eigenvalues or frequencies. The modes corresponding to the three lowest frequencies are simulated. The external excitations or forcing functions driving these modes can also be expanded in terms of the same eigenfunctions. Since all of the excitations are modelled by forces applied at a point, they are all spatial impulses. The expansion of the driving functions thus becomes the vector inner product of the external force and the normalized deflection of the mode at the point of application of the force. The equation for the generalized coordinate for a given bending mode with the driving terms included is

$$D^2QB_J/DT^2 = -2 ZETAB_J WB_J D QB_J/DT - WB_J^2 QB_J + \sum_I (DISP_I/GM) \cdot FORCE_I$$

pitch and yaw. Therefore, the angle between the thrust vector direction and the vehicle axis will be the sum of the engine angular position and the engine mount angular offset. Angular positions are measured as positive rotations of the engine about the vehicle Y and Z axes (e. g. a positive engine angular position in pitch will result in a negative pitch acceleration of the vehicle).

Optics D/A limit (optics error counter)	LMP	384	pulses	
Scale factor: pulse count to gimbal angle command	RPP	1.42	arc min per pulse	8/15/68
Pulse train rate	PPS	3200	pulses per sec	
Clutch torque limit	LMT	1300	ft lb	
Gimbal rate limit	LMR	0.15	rad/sec	
Gimbal position limit	LMG	4.5	deg	
Engine gimbal mounting offset-pitch	YBIAS	-2.15	deg	
Engine gimbal mounting offset-yaw	ZBIAS	0.95	deg	

6.4.7 CSM/LM Bending

It is necessary to simulate the structural deflections of the spacecraft caused by external loadings or contact forces such as main propulsion system thrust, RCS thrust, and fuel slosh. These structural deflections influence the spacecraft control systems by deflecting the navigation base. The bending deflection of the spacecraft can be expanded in terms of an infinite number of orthogonal eigenfunctions or modes and their associated eigenvalues or frequencies. The modes corresponding to the three lowest frequencies are simulated. The external excitations or forcing functions driving these modes can also be expanded in terms of the same eigenfunctions. Since all of the excitations are modelled by forces applied at a point, they are all spatial impulses. The expansion of the driving functions thus becomes the vector inner product of the external force and the normalized deflection of the mode at the point of application of the force. The equation for the generalized coordinate for a given bending mode with the driving terms included is

$$D^2QB_J/DT^2 = -2 ZETAB_J WB_J D QB_J/DT - WB_J^2 QB_J + \sum_I (DISP_I/GM) \cdot FORCE_I$$

6-27a

Revised COLOSSUS

Added GSOP # R-577 PCR # 624 Rev. 1 Date 12/68

where QB_J is the generalized coordinate associated with the Jth mode,
 $ZETAB_J$ is the damping ratio associated with the Jth mode,
 WB_J is the frequency associated with the Jth mode,
 $FORCE_I$ is one of the contact forces which excite the generalized bending coordinates,
 $DISP_I$ is the vector displacement of the point of application of $FORCE_I$,
 GM is the generalized mass associated with the Jth mode.

It is seen that the bending coordinate for each of the three simulated modes is the solution of a second-order differential equation.

The motion of the navigation base is the product of the modal displacements at the navigation base and the appropriate derivative of the generalized bending coordinate. For example, the translational velocity of the navigation base due to the Jth bending mode is given by

$$\underline{V}_J = \underline{DISPNB}_J D QB_J / DT$$

where \underline{DISPNB}_J is the modal displacement of the navigation base due to the Jth bending mode.

Similarly, rotational displacement of the navigation base is the product of a modal rotation vector at the navigation base and the generalized bending coordinate

$$\underline{\theta} = \underline{SLOPNB}_J QB_J$$

where \underline{SLOPNB}_J is the modal rotation of the navigation base due to the Jth bending mode.

The mode shapes, or specifically the displacements and rotations at individual spacecraft stations and the corresponding modal frequencies, depend on the mass distribution of the spacecraft. Data are thus required for representative loading conditions. The data are the displacements and rotations at all points of interest given below, the generalized mass, and the frequency and damping ratio for each mode. Three complete sets of data are given, one for each reference vehicle mass. A linear interpolation based on instantaneous total vehicle mass is used to obtain the bending parameters at points between two adjacent reference masses. Within a set of data for a given reference mass, each parameter has three entries for a scalar parameter, or nine entries for a vector parameter.

The first entry for a scalar parameter, or the first three entries for a vector parameter, pertain to the first mode simulated; the second or second three pertain to the second mode simulated; and similarly for the third mode. The vector parameters are expressed in the Apollo coordinate system.

Bending Data

The following data are expressed in the Apollo coordinate system:

<u>SPS 100%</u>			4.10
Reference spacecraft mass	MB ₀	91590	lb
SPS propellant loading 100%			
DPS propellant loading 100%			
APS propellant loading 100%			
Generalized mass used for modes	GM	1.0	lb sec ² /in.
Frequency of each mode	RWB1 ₀	2.08	cps
	RWB2 ₀	2.26	cps
	RWB3 ₀	2.44	cps
Damping ratio for generalized coordinate	ZETA1	0.005	nd
	ZETA2	0.005	nd
	ZETA3	0.005	nd
Displacement of the SPS trim gimbal station	RDSPT1 ₀	-0.00353	in./in.
		0.03294	in./in.
		0.06023	in./in.
	RDSPT2 ₀	-0.00093	in./in.
		0.05176	in./in.
		-0.03372	in./in.
	RDSPT3 ₀	-0.00205	in./in.
		0.02919	in./in.
		-0.01589	in./in.
Rotation of the SPS trim gimbal station	RROTT1 ₀	0.0	rad/in.
		0.0006605	rad/in.
		-0.0003967	rad/in.
	RROTT2 ₀	0.0	rad/in.
		-0.0003741	rad/in.
		-0.0006000	rad/in.

	RROTT3 ₀	0.0	rad/in.
		-0.0001041	rad/in.
		-0.0002658	rad/in.
Displacement of SM RCS Quad A	RDSPR1 ₀	-0.05799	in./in.
		-0.02290	in./in.
		-0.02407	in./in.
	RDSPR2 ₀	0.02244	in./in.
		-0.04816	in./in.
		0.02085	in./in.
	RDSPR3 ₀	0.00478	in./in.
		-0.05992	in./in.
		-0.01277	in./in.
Displacement of SM RCS Quad B	RDSPR1 ₃	0.01271	in./in.
		-0.01703	in./in.
		-0.03238	in./in.
	RDSPR2 ₃	0.04857	in./in.
		-0.02949	in./in.
		-0.00539	in./in.
	RDSPR3 ₃	0.02106	in./in.
		0.00854	in./in.
		0.06136	in./in.
Displacement of SM RCS Quad C	RDSPR1 ₆	0.05016	in./in.
		-0.00802	in./in.
		-0.02614	in./in.
	RDSPR2 ₆	-0.02440	in./in.
		-0.00152	in./in.
		0.01319	in./in.
	RDSPR3 ₆	-0.00516	in./in.
		-0.07158	in./in.
		0.00628	in./in.

Displacement of SM RCS Quad D	RDSPR1 ₉	-0.02032	in./in.
		-0.01388	in./in.
		-0.01775	in./in.
	RDSPR2 ₉	-0.05100	in./in.
		-0.01993	in./in.
		0.03995	in./in.
	RDSPR3 ₉	-0.02164	in./in.
		-0.02109	in./in.
		-0.06587	in./in.
Displacement of CSM navigation base	RDSPA1 ₀	0.0	in./in.
		-0.05300	in./in.
		-0.09059	in./in.
	RDSPA2 ₀	0.0	in./in.
		-0.08607	in./in.
		0.05610	in./in.
	RDSPA3 ₀	0.0	in./in.
		-0.02992	in./in.
		0.00766	in./in.
Rotation of CSM navigation base	RROTA1 ₀	0.0000249	rad/in.
		0.0005974	rad/in.
		-0.0003090	rad/in.
	RROTA2 ₀	0.0000530	rad/in.
		-0.0003347	rad/in.
		-0.0004559	rad/in.
	RROTA3 ₀	0.0000916	rad/in.
		-0.0000598	rad/in.
		-0.0002428	rad/in.
Displacement of top of oxidizer storage tank	RDSP01 ₀	0.0	in./in.
		-0.01127	in./in.
		-0.02700	in./in.
	RDSP02 ₀	0.0	in./in.
		-0.00305	in./in.
		0.00218	in./in.
	RDSP03 ₀	0.0	in./in.
		-0.05988	in./in.
		0.02288	in./in.

Displacement of top of fuel storage tank	RDSPF1 ₀	0.0	in./in.	
		-0.02305	in./in.	
		0.0	in./in.	
	RDSPF2 ₀	0.0	in./in.	
		-0.03960	in./in.	
		0.0	in./in.	
	RDSPF3 ₀	0.0	in./in.	
		0.04885	in./in.	
		0.0	in./in.	
<u>SPS 50%</u>				4.11
Reference spacecraft mass	MB ₁	76098.0	lb	
SPS propellant loading 50%				
DPS propellant loading 100%				
APS propellant loading 100%				
Generalized mass used for all modes	GM	1.0	lb sec ² /in.	
Frequency of each mode	RWB1 ₁	2.20	cps	
	RWB2 ₁	2.32	cps	
	RWB3 ₁	2.47	cps	
Damping ratio for generalized coordinate	ZETA1	0.005	nd	
	ZETA2	0.005	nd	
	ZETA3	0.005	nd	
Displacement of the SPS trim gimbal station	RDSPT1 ₃	-0.00323	in./in.	
		0.05206	in./in.	
		0.06763	in./in.	
	RDSPT2 ₃	-0.00032	in./in.	
		0.05493	in./in.	
		-0.04736	in./in.	
	RDSPT3 ₃	-0.00291	in./in.	
		0.02716	in./in.	
		-0.03091	in./in.	

Displacement of top of fuel storage tank	RDSPF1 ₀	0.0	in./in.	
		-0.02305	in./in.	
		-0.0212	in./in.	8/15/68
	RDSPF2 ₀	0.0	in./in.	
		-0.03960	in./in.	
		0.0204	in./in.	8/15/68
	RDSPF3 ₀	0.0	in./in.	
		0.04885	in./in.	
		-0.0299	in./in.	8/15/68
				4.11
<u>SPS 50%</u>				
Reference spacecraft mass	MB ₁	76098.0	lb	
SPS propellant loading 50%				
DPS propellant loading 100%				
APS propellant loading 100%				
Generalized mass used for all modes	GM	1.0	lb sec ² /in.	
Frequency of each mode	RWB1 ₁	2.20	cps	
	RWB2 ₁	2.32	cps	
	RWB3 ₁	2.47	cps	
Damping ratio for generalized coordinate	ZETA1	0.005	nd	
	ZETA2	0.005	nd	
	ZETA3	0.005	nd	
Displacement of the SPS trim gimbal station	RDSPT1 ₃	-0.00323	in./in.	
		0.05206	in./in.	
		0.06763	in./in.	
	RDSPT2 ₃	-0.00032	in./in.	
		0.05493	in./in.	
		-0.04736	in./in.	
	RDSPT3 ₃	-0.00291	in./in.	
		0.02716	in./in.	
		-0.03091	in./in.	

6-32a

Revised COLOSSUS

Added GSOP # R-577 PCR # 624 Rev. 1 Date 12/68

Rotation of the SPS trim gimbal station	RROTT1 ₃	0.0	rad/in.
		0.0006589	rad/in.
		-0.0005334	rad/in.
	RROTT2 ₃	0.0	rad/in.
		-0.0005074	rad/in.
		-0.0005929	rad/in.
	RROTT3 ₃	0.0	rad/in.
		-0.0001947	rad/in.
		-0.0001726	rad/in.
Displacement of SM RCS Quad A	RDSPR1 ₁₂	-0.05872	in./in.
		-0.02396	in./in.
		-0.01536	in./in.
	RDSPR2 ₁₂	0.03226	in./in.
		-0.03864	in./in.
		0.02238	in./in.
	RDSPR3 ₁₂	0.01223	in./in.
		0.06315	in./in.
		-0.01714	in./in.
Displacement of SM RCS Quad B	RDSPR1 ₁₅	0.02336	in./in.
		-0.01643	in./in.
		-0.02617	in./in.
	RDSPR2 ₁₅	0.04867	in./in.
		-0.02193	in./in.
		-0.00085	in./in.
	RDSPR3 ₁₅	0.02092	in./in.
		0.01154	in./in.
		0.05702	in./in.
Displacement of SM RCS Quad C	RDSPR1 ₁₈	0.05175	in./in.
		-0.00507	in./in.
		-0.01818	in./in.
	RDSPR2 ₁₈	-0.03367	in./in.
		0.00244	in./in.
		0.01516	in./in.
	RDSPR3 ₁₈	-0.01148	in./in.
		-0.06690	in./in.
		0.00443	in./in.

Displacement of SM RCS Quad D	RDSPR1 ₂₁	-0.03039	in./in.
		-0.01239	in./in.
		-0.00766	in./in.
	RDSPR2 ₂₁	-0.05074	in./in.
		-0.01386	in./in.
		0.03896	in./in.
	RDSPR3 ₂₁	-0.01968	in./in.
		-0.01561	in./in.
		-0.06943	in./in.
Displacement of CSM navigation base	RDSPA1 ₃	0.0	in./in.
		-0.06534	in./in.
		-0.08270	in./in.
	RDSPA2 ₃	0.0	in./in.
		-0.07594	in./in.
		0.07016	in./in.
	RDSPA3 ₃	0.0	in./in.
		-0.02573	in./in.
		0.01194	in./in.
Rotation of CSM navigation base	RROTA1 ₃	0.0000106	rad/in.
		0.0006027	rad/in.
		-0.0004267	rad/in.
	RROTA2 ₃	0.0000347	rad/in.
		-0.0004461	rad/in.
		-0.0004399	rad/in.
	RROTA3 ₃	0.0001466	rad/in.
		-0.0001436	rad/in.
		-0.0002133	rad/in.
Displacement of bottom of oxidizer storage tank	RDSP01 ₃	0.03585	in./in.
		0.04506	in./in.
		0.04952	in./in.
	RDSP02 ₃	-0.01677	in./in.
		0.05439	in./in.
		-0.04047	in./in.

	RDSPO3 ₃	-0.00654	in./in.	
		-0.02075	in./in.	
		-0.01019	in./in.	
Displacement of top of oxidizer sump tank	RDSPO1 ₆	0.0	in./in.	
		-0.01394	in./in.	
		-0.02394	in./in.	
	RDSPO2 ₆	0.0	in./in.	
		-0.00302	in./in.	
		-0.02737	in./in.	
RDSPO3 ₆	0.0	in./in.		
	-0.04017	in./in.		
	0.11774	in./in.		
Displacement of bottom of fuel storage tank	RDSPF1 ₃	-0.04272	in./in.	
		0.03277	in./in.	
		0.05352	in./in.	
	RDSPF2 ₃	0.01573	in./in.	
		0.02748	in./in.	
		-0.03098	in./in.	
	RDSPF3 ₃	0.00459	in./in.	
		0.06547	in./in.	
		-0.04117	in./in.	
	Displacement of top of fuel sump tank	RDSPF1 ₆	0.0	in./in.
			0.01943	in./in.
			-0.00229	in./in.
RDSPF2 ₆		0.0	in./in.	
		-0.02241	in./in.	
		0.03738	in./in.	
RDSPF3 ₆		0.0	in./in.	
		0.02947	in./in.	
		-0.10876	in./in.	

	RDSP03 ₃	-0.00654	in./in.	
		-0.02075	in./in.	
		-0.01019	in./in.	
Displacement of top of oxidizer sump tank	RDSP01 ₆	0.0	in./in.	
		-0.01394	in./in.	
		-0.02394	in./in.	
	RDSP02 ₆	0.0	in./in.	
		-0.00302	in./in.	
		-0.02737	in./in.	
Displacement of bottom of fuel storage tank	RDSP03 ₆	0.0	in./in.	
		-0.04017	in./in.	
		0.11774	in./in.	
	RDSPF1 ₃	-0.04272	in./in.	
		0.03277	in./in.	
		0.05352	in./in.	
Displacement of top of fuel sump tank	RDSPF2 ₃	0.01573	in./in.	
		0.02748	in./in.	
		-0.03098	in./in.	
	RDSPF3 ₃	0.00459	in./in.	
		0.06547	in./in.	
		-0.04117	in./in.	
Displacement of top of fuel sump tank	RDSPF1 ₆	0.0	in./in.	
		-0.01943	in./in.	8/15/68
		-0.00229	in./in.	
	RDSPF2 ₆	0.0	in./in.	
		-0.02241	in./in.	
		0.03738	in./in.	
Displacement of top of fuel sump tank	RDSPF3 ₆	0.0	in./in.	
		0.02947	in./in.	
		-0.10876	in./in.	

6-35 a

Revised COLOSSUS

Added GSOP #R-577 PCR # 624 Rev. 1 Date 12/68

SPS 25%

4.12

Reference spacecraft mass	MB ₂	65915.0	lb
SPS propellant loading 25%			
DPS propellant loading 100%			
APS propellant loading 100%			
Generalized mass used for all modes	GM	1.0	lb sec ² /in.
Frequency of each mode	RWB1 ₂	2.24	cps
	RWB2 ₂	2.38	cps
	RWB3 ₂	2.97	cps
Damping ratio for generalized coordinate	ZETA1	0.005	nd
	ZETA2	0.005	nd
	ZETA3	0.005	nd
Displacement of the SPS trim gimbal station	RDSPT1 ₆	-0.00266	in./in.
		0.04405	in./in.
		0.08190	in./in.
	RDSPT2 ₆	-0.00176	in./in.
		0.07629	in./in.
		-0.04505	in./in.
	RDSPT3 ₆	-0.00051	in./in.
		0.01436	in./in.
		-0.01101	in./in.
Rotation of the SPS trim gimbal station	RROTT1 ₆	0.0	rad/in.
		0.0007691	rad/in.
		-0.0004293	rad/in.
	RROTT2 ₆	0.0	rad/in.
		-0.0004182	rad/in.
		-0.0007434	rad/in.
	RROTT3 ₆	0.0	rad/in.
		-0.0000629	rad/in.
		-0.0000738	rad/in.

Displacement of SM RCS Quad A	RDSPR1 ₂₄	-0.06537	in./in.
		-0.01482	in./in.
		-0.01620	in./in.
	RDSPR2 ₂₄	0.02334	in./in.
		-0.02886	in./in.
		0.01199	in./in.
	RDSPR3 ₂₄	0.00376	in./in.
		0.13613	in./in.
		-0.02382	in./in.
Displacement of SM RCS Quad B	RDSPR1 ₂₇	0.01508	in./in.
		-0.01087	in./in.
		-0.02198	in./in.
	RDSPR2 ₂₇	0.05856	in./in.
		-0.01940	in./in.
		-0.00104	in./in.
	RDSPR3 ₂₇	0.00808	in./in.
		0.03249	in./in.
		0.12585	in./in.
Displacement of SM RCS Quad C	RDSPR1 ₃₀	0.05987	in./in.
		-0.00471	in./in.
		-0.01743	in./in.
	RDSPR2 ₃₀	-0.02573	in./in.
		-0.00576	in./in.
		0.00810	in./in.
	RDSPR3 ₃₀	-0.00333	in./in.
		-0.12959	in./in.
		0.01536	in./in.
Displacement of SM RCS Quad D	RDSPR1 ₃₃	-0.02053	in./in.
		-0.00850	in./in.
		-0.01199	in./in.
	RDSPR2 ₃₃	-0.06159	in./in.
		-0.01479	in./in.
		0.02140	in./in.
	RDSPR3 ₃₃	-0.00707	in./in.
		-0.02628	in./in.
		-0.13280	in./in.

Displacement of CSM navigation base	RDSPA1 ₆	0.0	in./in.
		-0.05080	in./in.
		-0.09383	in./in.
	RDSPA2 ₆	0.0	in./in.
		-0.08990	in./in.
		0.05206	in./in.
	RDSPA3 ₆	0.0	in./in.
		-0.03293	in./in.
		0.00192	in./in.
Rotation of CSM navigation base	RROTA1 ₆	0.0000022	rad/in.
		0.0007058	rad/in.
		-0.0003570	rad/in.
	RROTA2 ₆	0.0000263	rad/in.
		-0.0003618	rad/in.
		-0.0005890	rad/in.
	RROTA3 ₆	0.0008182	rad/in.
		-0.0000247	rad/in.
		-0.0001058	rad/in.
Displacement of middle of oxidizer sump tank	RDSP01 ₉	0.0	in./in.
		0.01115	in./in.
		0.02245	in./in.
	RDSP02 ₉	0.0	in./in.
		0.02324	in./in.
		-0.02394	in./in.
	RDSP03 ₉	0.0	in./in.
		-0.00777	in./in.
		0.09164	in./in.
Displacement of middle of fuel sump tank	RDSPF1 ₉	0.0	in./in.
		0.01030	in./in.
		0.02875	in./in.
	RDSPF2 ₉	0.0	in./in.
		0.02036	in./in.
		-0.00725	in./in.
	RDSPF3 ₉	0.0	in./in.
		0.02426	in./in.
		-0.10382	in./in.

6.4.8 Propellant Slosh

4.2

Slosh motions of the propellant in the SPS tanks are simulated as a linear spring mass system. Each tank in which sloshing occurs is characterized by a slosh mass, a slosh frequency and a slosh mass attachment point. Slosh mass motion is constrained to the plane defined by the vehicle Y and Z axes. Sloshing occurs either in the two storage tanks (no slosh in the full sump tanks) or in the two sump tanks (no slosh in the empty storage tanks). It is assumed, for each tank, that slosh mass is constant, slosh frequency is inversely proportional to the square root of vehicle mass, and the X coordinate of the slosh attachment point varies linearly with propellant mass. Slosh damping ratios are held constant.

6.4.8.1 Slosh dynamics

Oxidizer storage tank slosh mass	MO_0	24.95	slugs
Fuel storage tank slosh mass	MF_0	15.61	slugs
Oxidizer sump tank slosh mass	MO_1	35.85	slugs
Fuel sump tank slosh mass	MF_1	22.43	slugs
Oxidizer storage tank slosh frequency	WO_0	3.40	rad/sec
Fuel storage tank slosh frequency	WF_0	3.40	rad/sec
Vehicle mass corresponding to storage tank slosh frequencies	MP_0	59901.0	lb
Oxidizer sump tank slosh frequency	WO_1	3.88	rad/sec
Full sump tank slosh frequency	WF_1	3.88	rad/sec
Vehicle mass corresponding to sump tank slosh frequencies	MP_1	40588.0	lb

Oxidizer slosh damping ratio	ZETAO	0.0007	nd
Fuel slosh damping ratio	ZETAF	0.0007	nd

6.4.8.2 Slosh Mass Attachment Point Locations

Oxidizer storage tank (full) slosh station (X_A coordinate)	XO ₀	933.7	in.
Fuel storage tank (full) slosh station (X_A coordinate)	XF ₀	933.0	in.
Propellant mass corresponding to full storage tanks	MX ₀	38626.0	lb
Oxidizer storage tank (half) slosh station (X_A coordinate)	XO ₁	862.0	in.
Fuel storage tank (half) slosh station (X_A coordinate)	XF ₁	861.7	in.
Propellant mass corresponding to half-full storage tanks	MX ₁	28969.0	lb
Oxidizer sump tank (full slosh station) (X_A coordinate)	XO ₂	922.5	in.
Fuel sump tank (full) slosh station (X_A coordinate)	XF ₂	922.3	in.
Propellant mass corresponding to full sump tanks	MX ₂	19313.0	lb
Oxidizer sump tank (half) slosh station (X_A coordinate)	XO ₃	869.1	in.

Fuel sump tank (half) slosh station (X_A coordinate)	XF_3	869.0	in.
Propellant mass corresponding to half full sump tanks	MX_3	10043.0	lb
Oxidizer storage tank Y coordinate (Y_A coordinate)	YO_0	14.8	in.
Fuel storage tank Y coordinate (Y_A coordinate)	YF_0	-14.8	in.
Oxidizer sump tank Y coordinate (Y_A coordinate)	YO_1	48.3	in.
Fuel sump tank Y coordinate (Y_A coordinate)	YF_1	-48.3	in.
Oxidizer storage tank Z coordinate (Z_A coordinate)	ZO_0	47.8	in.
Fuel storage tank Z coordinate (Z_A coordinate)	ZF_0	-47.8	in.
Oxidizer sump tank Z coordinate (Z_A coordinate)	ZO_1	6.6	in.
Fuel sump tank Z coordinate (Z_A coordinate)	ZF_1	-6.6	in.
Apollo station of tank bottoms	XTB	832.0	in.

6.5 Digital Simulator CM (CM-103) Reentry Spacecraft Data

6.5.1 CM Reference Positions and Dimensions

The following reference positions and dimensions are expressed in the CM vehicle coordinate system in the order X component, Y component, Z component, unless otherwise noted.

6.5.1.1	CM Navigation Base	RNB	55.715	in.	5.1
	Position		0.0	in.	
			40.914	in.	
6.5.1.2	CM RCS Thruster Positions				5.2
	Jet 1		27.6750	in.	
			4.4211	in.	
			-72.2846	in.	
	Jet 2		85.1200	in.	
			3.929	in.	
			-35.5743	in.	
	Jet 3		27.6750	in.	
			-4.4211	in.	
			-72.2846	in.	
	Jet 4		85.1200	in.	
			-3.929	in.	
			-35.5743	in.	
	Jet 5		27.6750	in.	
			72.2846	in.	
			-4.4211	in.	
	Jet 6		27.6750	in.	
			-72.2846	in.	
			-4.4211	in.	
	Jet 7		27.6750	in.	
			72.2846	in.	
			4.4211	in.	
	Jet 8		27.6750	in.	
			-72.2846	in.	
			4.4211	in.	

Jet 9	32.3000 in.
	51.9826 in.
	-50.3454 in.
Jet 10	32.3000 in.
	-51.9826 in.
	-50.3454 in.
Jet 11	32.3000 in.
	-51.9826 in.
	-50.3454 in.
Jet 12	32.3000 in.
	51.9826 in.
	-50.3454 in.

6.5.2 CM Mass Properties

5.3

At present, the entry simulation does not account for changes in CM mass properties due to RCS propellant usage or heat shield ablator loss. Hence, the mass, center of gravity, and inertia of the vehicle are assumed constant during the simulated entry at values corresponding to CM/SM separation. The center of gravity is expressed in the CM vehicle coordinate system. The moments and products of inertia are about the vehicle center of gravity and with respect to the CM vehicle axes. Both the diagonal and off-diagonal elements of the inertia tensor are used as positive elements. Hence the numerical values of the off-diagonal elements reported below have signs opposite to those given in the referenced document.

Mass		MASS	12984	lb
Center of Gravity	X	CG_0	41.7	in.
	Y		-0.4	in.
	Z		5.6	in.
Inertia	I_{XX}	$INERTIA_0$	6068.0	slug ft ²
	I_{XY}		-62.3	slug ft ²
	I_{XZ}		434.4	slug ft ²
	I_{YX}		-62.3	slug ft ²
	I_{YY}		5431.0	slug ft ²
	I_{YZ}		-12.0	slug ft ²
	I_{ZX}		434.4	slug ft ²
	I_{ZY}		-12.0	slug ft ²
	I_{ZZ}		4883.0	slug ft ²

Jet 9	32.3000 in.
	51.9826 in.
	-50.3454 in.
Jet 10	32.3000 in.
	-51.9826 in.
	-50.3454 in.
Jet 11	32.3000 in.
	-51.9826 in.
	-50.3454 in.
Jet 12	32.3000 in.
	51.9826 in.
	-50.3454 in.

6.5.2 CM Mass Properties

5.3

At present, the entry simulation does not account for changes in CM mass properties due to RCS propellant usage or heat shield ablator loss. Hence, the mass, center of gravity, and inertia of the vehicle are assumed constant during the simulated entry at values corresponding to CM/SM separation. The center of gravity is expressed in the CM vehicle coordinate system. The moments and products of inertia are about the vehicle center of gravity and with respect to the CM vehicle axes. Both the diagonal and off-diagonal elements of the inertia tensor are used as positive elements. Hence the numerical values of the off-diagonal elements reported below have signs opposite to those given in the referenced document.

Mass		MASS	12215.8	lb	9/30/68
Center of Gravity	X	CG ₀	40.7	in.	9/30/68
	Y		0.0	in.	9/30/68
	Z		5.9	in.	9/30/68
Inertia	I _{XX}	INERTIA ₀	5817.0	slug ft ²	9/30/68
	I _{XY}		-46.6	slug ft ²	9/30/68
	I _{XZ}		403.0	slug ft ²	9/30/68
	I _{YX}		-46.6	slug ft ²	9/30/68
	I _{YY}		4985.0	slug ft ²	9/30/68
	I _{YZ}		-27.4	slug ft ²	9/30/68
	I _{ZX}		403.0	slug ft ²	9/30/68
	I _{ZY}		-27.4	slug ft ²	9/30/68
	I _{ZZ}		4506.0	slug ft ²	9/30/68

6-43a

Revised COLOSSUS

Added GSOP # R-577 PCR # 629 Rev. 1 Date 12/68

The individual RCS thruster is modelled as a constant thrust, constant specific impulse motor; values of thrust and specific impulse presented below correspond to the nominal vacuum performance of the basic thruster with no nozzle extension, i. e. , prior to installation in the command module. The performance of an engine installed in the spacecraft will vary from location to location, depending upon the geometry of the nozzle extension for that particular location. The average increase in steady-state axial thrust and specific impulse from the addition of various nozzle extensions is also given below. It is noted that the addition of a nozzle extension will have no effect on the steady-state or pulse mode propellant flow rates or mixture ratios.

No provision is made in the entry simulation to account for the falloff of thrust with increasing atmospheric pressure. The buildup and tailoff of thrust are modelled by instantaneous changes in thrust, shifted in time from the electrical command. The shift is different for the application and removal of thrust. The amount of the shift is calculated to give the same total impulse during a transient firing as would be obtained from a real thruster.

6.5.3.1 Thrust	TH	93.6	lb
Specific Impulse	RCISP	272.1	sec
Step delay in RCS thrust application from receipt of electrical command	RCONDEL	0.012	sec
Step delay in RCS thrust removal from receipt of electrical command	RCOFFDEL	0.007	sec
Minimum allowed RCS electrical pulse length	TMINPULS	0.014	sec
Thrust increase for pitch nozzle extension	ADTHRUST _P	2.1	lb
Thrust increase for yaw nozzle extension	ADTHRUST _Y	1.8	lb
Thrust increase for long roll nozzle extension	ADTHRUST _{LR}	0.6	lb
Thrust increase for short roll nozzle extension	ADTHRUST _{SR}	0.0	lb

Increase in specific impulse for pitch nozzle extention	ADISP _P	6.12	sec
Increase in specific impulse for yaw nozzle extention	ADISP _Y	5.24	sec
Increase in specific impulse for long roll nozzle extention	ADISP _{LR}	1.75	sec
Increase in specific impulse for short roll nozzle extention	ADISP _{SR}	0.0	sec

6.5.3.2 The direction of the thrust vectors produced by individual RCS thrusters can be obtained from Fig. 4-20 of the cited reference which shows the orientation of the individual thrust chamber center lines.

6.5.3.3 The propellant usage of each RCS thruster is modelled by a constant mass flow rate when the jet is firing plus a propellant penalty for each jet firing. The mass flow rate is calculated as follows:

$$RCMFLO = TH / (RCISP \cdot GRAV)$$

where GRAV is acceleration of gravity (32.174048 ft/sec²).

Propellant penalty per jet firing	NFIRTOKG	0.003	lb
-----------------------------------	----------	-------	----

6.5.4 CM Entry Aerodynamics

The CM lift-to-drag ratio (L/D) is not an explicit variable in the entry simulation; its value is implied, however, by the specification of a CM center of gravity location. Provision has been made to simulate the CM operating at an off-nominal L/D by varying the position of the CG along the spacecraft Z axis. CG position along the X and Y axes are assumed to remain constant, and the desired L/D is converted into a corresponding Z coordinate using a set of curves (Fig. 6.2, Ref. 5.3) which are analytically represented in the simulation. It is further assumed that the CG can be varied without causing variations in the nominal mass and inertia properties

of the vehicle. Although this cannot be done in actuality, no method is presently available for determining the variations that would occur and so they have not been accounted for.

The aerodynamic forces and moments acting on the CM during entry are calculated from three aerodynamic coefficients;

Force coefficient along the command module axis	CA
Force coefficient normal to the command module axis	CN
Pitching moment coefficient about the theoretical command module cone apex	CM

Values of the aerodynamic coefficients are presented at three angles of attack for each of eleven Mach numbers. Values at other angles of attack and Mach numbers are found by a parabolic interpolation between the three tabulated angles and by a linear interpolation between the two nearest reference Mach numbers. The data has been corrected for an effective aft heat shield cant of 0.1365 degrees and centerline shift in the +Z direction.

6.5.4.1

Lift-to-Drag Ratio	LDNOM	0.283	nd	5.3
Reference Mach numbers for interpolation	MACHD ₀	6.0	nd	5.3
		3.0	nd	
		2.4	nd	
		2.0	nd	
		1.65	nd	
		1.35	nd	
		1.2	nd	
		1.1	nd	
		0.9	nd	
		0.7	nd	
		0.4	nd	
Reference angles of attack for interpolation	REFALPH ₀	140.1365	deg	5.3
		160.1365	deg	
		180.1365	deg	

of the vehicle. Although this cannot be done in actuality, no method is presently available for determining the variations that would occur and so they have not been accounted for.

The aerodynamic forces and moments acting on the CM during entry are calculated from three aerodynamic coefficients:

Force coefficient along the command module axis	CA
Force coefficient normal to the command module axis	CN
Pitching moment coefficient about the theoretical command module cone apex	CM

Values of the aerodynamic coefficients are presented at three angles of attack for each of eleven Mach numbers. Values at other angles of attack and Mach numbers are found by a parabolic interpolation between the three tabulated angles and by a linear interpolation between the two nearest reference Mach numbers. The data has been corrected for an effective aft heat shield cant of 0.1365 degrees and centerline shift in the +Z direction.

6.5.4.1

Lift-to-Drag Ratio	LDNOM	0.296	nd	10/1/68	5.3
Reference Mach numbers for interpolation	MACHD ₀	6.0	nd		5.3
		3.0	nd		
		2.4	nd		
		2.0	nd		
		1.65	nd		
		1.35	nd		
		1.2	nd		
		1.1	nd		
		0.9	nd		
		0.7	nd		
		0.4	nd		
Reference angles of attack for interpolation	REFALPH ₀	140.1365	deg		5.3
		160.1365	deg		
		180.1365	deg		

6-46a

Revised COLOSSUS

Added GSOP # R-577 PCR # 629 Rev. 1 Date 12/68

Moment reference center (CM theoretical apex)	REF ₀	141.25 0.0 0.0	in. in. in.	5.2
Reference area for converting aerodynamic coefficients to forces and moments	AREA	129.35	ft ²	5.2
Reference length for converting pitching moment coefficient to pitching moment	REFD	154.0	in.	5.2
6.5.4.2 Tabulated Values of Aerodynamic Coefficients				5.2

Hypersonic Mach Range (6-25)

ALPHA = 140.1365 deg	CM	-0.0328
	CN	0.1687
	CA	-0.9794
ALPHA = 160.1365 deg	CM	0.0033
	CN	0.0748
	CA	-1.3452
ALPHA = 180.1365 deg	CM	0.0137
	CN	-0.0035
	CA	-1.4900

Mach 3.0

ALPHA = 140.1365 deg	CM	-0.0576
	CN	0.1875
	CA	-1.0304
ALPHA = 160.1365 deg	CM	-0.0036
	CN	0.0697
	CA	-1.3802
ALPHA = 180.1365 deg	CM	0.0057
	CN	-0.0035
	CA	-1.4750

	<u>Mach</u>	<u>2.4</u>
ALPHA = 140.1365 deg	CM	-0.0644
	CN	0.1974
	CA	-1.0805
ALPHA = 160.1365 deg	CM	0.0026
	CN	0.0587
	CA	-1.4051
ALPHA = 180.1365 deg	CM	0.0057
	CN	-0.0035
	CA	-1.4700

	<u>Mach</u>	<u>2.0</u>
ALPHA = 140.1365 deg	CM	-0.0683
	CN	0.2024
	CA	-1.1055
ALPHA = 160.1365 deg	CM	0.0108
	CN	0.0466
	CA	-1.4361
ALPHA = 180.1365 deg	CM	0.0057
	CN	-0.0035
	CA	-1.4720

	<u>Mach</u>	<u>1.65</u>
ALPHA = 140.1365 deg	CM	-0.0659
	CN	0.2042
	CA	-1.1805
ALPHA = 160.1365 deg	CM	0.0132
	CN	0.0416
	CA	-1.4201
ALPHA = 180.1365 deg	CM	0.0056
	CN	-0.0035
	CA	-1.4500

	<u>Mach</u>	<u>1.35</u>
ALPHA = 140.1365 deg	CM	-0.0615
	CN	0.2071
	CA	-1.2205

ALPHA = 160.1365 deg	CM	0.0177
	CN	0.0367
	CA	-1.4051
ALPHA = 180.1365 deg	CM	0.0054
	CN	-0.0034
	CA	-1.4200
<u>Mach 1.2</u>		
ALPHA = 140.1365 deg	CM	-0.0232
	CN	0.1542
	CA	-1.1614
ALPHA = 160.1365 deg	CM	0.0164
	CN	-0.0370
	CA	-1.2801
ALPHA = 180.1365 deg	CM	0.0051
	CN	-0.0032
	CA	-1.3250
<u>Mach 1.1</u>		
ALPHA = 140.1365 deg	CM	-0.0142
	CN	0.1462
	CA	-1.1684
ALPHA = 160.1365 deg	CM	0.0189
	CN	0.0349
	CA	-1.2901
ALPHA = 180.1365 deg	CM	0.0050
	CN	-0.0031
	CA	-1.3050
<u>Mach 0.9</u>		
ALPHA = 140.1365 deg	CM	0.0313
	CN	0.0848
	CA	-0.9352
ALPHA = 160.1365 deg	CM	0.0233
	CN	0.0354
	CA	-1.1051
ALPHA = 180.1365 deg	CM	0.0042
	CN	-0.0026
	CA	-1.0900

	<u>Mach 0.7</u>	
ALPHA = 140.1365 deg	CM	0.0859
	CN	0.0280
	CA	-0.8601
ALPHA = 160.1365 deg	CM	0.0304
	CN	0.0276
	CA	-1.0001
ALPHA = 180.1365 deg	CM	0.0038
	CN	-0.0023
	CA	-0.9800

	<u>Mach 0.4</u>	
ALPHA = 140.1365 deg	CM	0.1049
	CN	-0.0118
	CA	-0.7400
ALPHA = 160.1365 deg	CM	0.1196
	CN	-0.0921
	CA	-0.8998
ALPHA = 180.1365 deg	CM	0.0034
	CN	-0.0021
	CA	-0.8700

6.6 Digital Simulator VHF Range System

The VHF range unit provides a range measurement to the CMC. Associated with this data interface is a "DATA GOOD" status signal. This status signal is generated by the simulator whenever the range unit is in use and the range to the LM is less than the specified limit given below. The issuance of this discrete by the simulator does not depend on the attitude of the CSM or LM.

Maximum range at which acquisition and tracking can occur	MAXR	370650	m	6.1
Range scale factor	RANGESC	0.053959261	bits/m	6.2

6.6 Digital Simulator VHF Range System

The VHF range unit provides a range measurement to the CMC. Associated with this data interface is a "DATA GOOD" status signal. This status signal is generated by the simulator whenever the range unit is in use and the range to the LM is less than the specified limit given below. The issuance of this discrete by the simulator does not depend on the attitude of the CSM or LM.

Maximum range at which acquisition and tracking can occur	MAXR	370650	m	6.1
Range scale factor	RANGESC	0.05399568	bits/m	6.2 8/30/68

6-51a

Revised COLOSSUS

Added GSOP #R-577 PCR # 624 Rev. 1 Date 12/68

6.7 Digital Simulator Coordinate Systems and Natural Environment Data

6.7.1 Reference Inertial Coordinate System

The reference inertial coordinate system used in verification of Apollo guidance computer programs is defined by the mean equator and mean equinox at the nearest beginning of a Besselian year. The rectangular coordinates are defined so that the +X axis is in the direction of the mean equinox, the +Z axis is along the mean rotational axis of the earth and the Y axis completes the right-handed set.

The origin of the reference system is the center of mass of the earth.

6.7.2 Geodetic Coordinate System

7.1

Positions in the earth-fixed system are specified by geodetic latitude, referenced to the Fischer ellipsoid of 1960; longitude, measured positive east from the meridian of Greenwich and altitude, measured above the ellipsoid along the geocentric radius vector.

A cross-section of the Fischer ellipsoid containing the axis of symmetry has the equation

$$(x^2/a^2) + (z^2/b^2) = 1$$

The equatorial radius of the earth	a	6378166	m
The flattening of the ellipsoid	(a-b)/a	1/298.3	n/a
The polar radius of the earth	b	6356784	m

6.7.3 Local Horizontal Coordinate System

The system to which spacecraft attitude is referenced is the local horizontal coordinate system. It is defined in terms of the spacecraft position and velocity expressed in the reference inertial coordinate system such that

$$\underline{u}_x = \underline{u}_y \times \underline{u}_z$$

$$\underline{u}_y = \underline{V}_{\text{ref}} \times \underline{R}_{\text{ref}} / |\underline{V}_{\text{ref}} \times \underline{R}_{\text{ref}}|$$

$$\underline{u}_z = -\underline{R}_{\text{ref}} / |\underline{R}_{\text{ref}}|$$

Starting with the vehicle coordinate axes initially aligned with the local horizontal system, the application of the Euler rotations pitch, yaw and roll about the Y, Z and X vehicle axes in that order determines the vehicle attitude.

6.7.4 Earth Gravitational Model

7.1

The gravitational potential of the earth is assumed to be

$$V_e(r, L) = (MU_e/r) \left[1 + (J/3) (r_e/r)^2 (1 - 3 \sin^2 L) \right. \\ \left. + (H/5) (r_e/r)^3 (3 - 5 \sin^2 L) \sin L \right. \\ \left. + (K/35) (r_e/r)^4 (3 - 30 \sin^2 L + 35 \sin^4 L) \right]$$

where r_e is the equatorial earth (gravitational) radius of the Fischer ellipsoid.

The earth's gravitational parameter	MU_e	3986032×10^8	m^3/sec^2
Oblateness coefficients	J	162345×10^{-8}	n/a
	H	-575×10^{-8}	n/a
	K	7875×10^{-9}	n/a

The mass distribution of the earth is assumed symmetric about the rotational axis, hence there is no dependence on longitude in the potential equation.

6.7.5 Sun and Moon Gravitational Models

7.1

The acceleration due to the sun and moon is the difference between the gravitational field at the spacecraft and the field at the origin of the coordinate system. The acceleration of the spacecraft due to the earth, sun, and moon relative to an inertial system is

$$\underline{a}_v = \underline{g}_e + (MU_s/r_{vs}^3) \underline{r}_{vs} + (MU_m/r_{vm}^3) \underline{r}_{vm}$$

The acceleration of the earth is

$$\underline{a}_e = (MU_s/r_{es}^3) \underline{r}_{es} + (MU_m/r_{em}^3) \underline{r}_{em}$$

Thus the acceleration of the vehicle relative to the center of mass of the earth is

$$\begin{aligned} \underline{a}_{ev} = \underline{g}_e + MU_s [(r_{vs}/r_{vs}^3) - (r_{es}/r_{es}^3)] \\ + MU_m [(r_{vm}/r_{vm}^3) - (r_{em}/r_{em}^3)] \end{aligned}$$

The sun's gravitational parameter	MU_s	132715445×10^{12}	m^3/sec^2
The moon's gravitational parameter	MU_m	4902778×10^6	m^3/sec^2

6.7.6 Atmospheric Model

7.2

The model of the earth's atmosphere is based on the 1962 U. S. Standard atmosphere; atmospheric perturbations due to winds are not included in the model. In the digital simulation, values of molecular scale temperature and density are tabulated for 14 reference altitudes ranging from 0 to 160,000 meters, and the temperature gradient between reference altitudes is also tabulated.

Using these reference data, atmospheric temperature T and density RHO at intermediate altitudes are calculated from the following equations:

Reference geopotentials and altitudes	BOUND ₀	160000 m
		150000 m
		120000 m
		110000 m
		100000 m
		90000 m
		79000 m
		61000 m
		52000 m
		47000 m
		32000 m
		20000 m
		11000 m
		0 m

Molecular scale temperatures at the reference altitudes	BTEMP ₀	1110.65	deg K
		960.65	deg K
		360.65	deg K
		260.65	deg K
		210.65	deg K
		180.65	deg K
		180.65	deg K
		252.65	deg K
		270.65	deg K
		270.65	deg K
		228.65	deg K
		216.65	deg K
		216.65	deg K
		288.15	deg K
Temperature gradients between reference altitudes	TEMPGRAD ₀	0.015	deg K/m
		0.020	deg K/m
		0.010	deg K/m
		0.005	deg K/m
		0.003	deg K/m
		0.0	deg K/m
		-0.004	deg K/m
		-0.002	deg K/m
		0.0	deg K/m
		0.0028	deg K/m
		0.001	deg K/m
		0.0	deg K/m
Densities at the reference altitudes	BRHO ₀	1159×10^{-12}	kg/m ³
		1836×10^{-12}	kg/m ³
		2436×10^{-11}	kg/m ³
		9829×10^{-11}	kg/m ³
		4974×10^{-10}	kg/m ³
		3170×10^{-9}	kg/m ³
		2001×10^{-8}	kg/m ³
		25109×10^{-8}	kg/m ³
		75943×10^{-8}	kg/m ³
		14275×10^{-7}	kg/m ³
		13225×10^{-6}	kg/m ³
		88035×10^{-6}	kg/m ³
		36392×10^{-5}	kg/m ³
		12250×10^{-4}	kg/m ³

Empirical constant used in atmospheric equations EARTH RAD 63550.00×10^2 m

$$ATMC = M_{AIR} \times G/R$$

$$SOUNDC = GAMMA \times R/M_{AIR}$$

Molecular weight of air	M_{AIR}	28.9644	n/a
Acceleration of gravity	G	9.80665	m/sec ²
Universal gas constant	R	8314.32	nm/kg K
Ratio of specific heats for air	GAMMA	1.4	n/a

Case 1: $H < BOUND_5$ (90,000 m)

$$K = (EARTH RAD \times H)/(EARTH RAD + H)$$

$$\Delta H_N = K - BOUND_N$$

If $TEMPGRAD_{N-1} = 0$, $T = BTEMP_N$

$$RHO = BRHO_N \exp(-ATMC \times \Delta H_N / BTEMP_N)$$

If $TEMPGRAD_{N-1} \neq 0$, $T = BTEMP_N + TEMPGRAD_{N-1} \times \Delta H_N$

$$RHO = BRHO_N \exp \left\{ (1 + ATMC / TEMPGRAD_{N-1}) \right.$$

$$\left. \times \ln [BTEMP_N / (BTEMP_N + TEMPGRAD_{N-1} \times \Delta H_N)] \right\}$$

Case 2: $H \geq \text{BOUND}_5$

$$\Delta H_N = H - \text{BOUND}_N$$

If $\text{TEMPGRAD}_{N-1} = 0$, $T = \text{BTEMP}_N$

$$\text{RHO} = \text{BRHO}_N \exp(-\text{ATMC} \times \Delta H_N / \text{BTEMP}_N)$$

If $\text{TEMPGRAD}_{N-1} \neq 0$, $T = \text{BTEMP}_N + \text{TEMPGRAD}_{N-1} \times \Delta H_N$

$$R_0 = 1 / (\text{EARTH RAD} + \text{BOUND}_N - \text{BTEMP}_N / \text{TEMPGRAD}_{N-1})$$

$$R_1 = \text{BTEMP}_N / (\text{BTEMP}_N + \text{TEMPGRAD}_{N-1} \times \Delta H_N)$$

$$R_2 = \Delta H_N / [(\text{EARTH RAD} + H) (\text{EARTH RAD} + \text{BOUND}_N)]$$

$$\text{RHO} = \text{BRHO}_N \exp \left\{ \text{ATMC} \times \text{EARTH RAD}^2 \times R_0 \right.$$

$$\times \left\{ R_2 + R_0 \ln [R_1 (1 + \Delta H_N / \text{EARTH RAD})] \right\} / \text{TEMPGRAD}_{N-1}$$

$$+ \ln R_1 \left. \right\}$$



Dynamic pressure Q and Mach number M can now be calculated as follows:

$$Q = 0.5 \text{ RHO} \left| \underline{\text{VAT}}_I \right|^2$$

where $\underline{\text{VAT}}_I$ is the velocity of the vehicle with respect to the atmosphere in the reference inertial coordinate system.

If $\text{RHO} \neq 0$,

$$M = \left| \underline{\text{VAT}}_I \right| / [\text{SOUNDC} (\text{BTEMP}_N + \text{TEMPGRAD}_{N-1} \times \Delta H_N)]^{1/2}$$

If $\text{RHO} = 0$, $M = 0$.

In the case that $H > \text{BOUND}_0$ (160,000 m), the simulation considers the vehicle to be "outside" the atmosphere, and sets Q and M equal to zero.

6.8 Hybrid Simulator Prelaunch Data

Intentionally Blank

No prelaunch environment is simulated.

6.9 Hybrid Simulator Launch Vehicle Data

Intentionally Blank

The launch vehicle is not simulated.

6.10 Hybrid Simulator CSM and LM Spacecraft Data

6.10.1 CSM Reference Positions and Dimensions

10.1

The following X, Y, and Z components describe positions in the Apollo Coordinate System. Inertias are about the center of gravity of each item.

6.10.1.1 CM Navigation Base	1055.715	in.
	0.0	in.
	40.914	in.
6.10.1.2 SPS Gimbal Ring	833.2	in.
	0.0	in.
	0.0	in.

6.10.1.3 SM RCS Positions and Orientation

The position vectors of the RCS jet thrust application points were modelled to have the same X component and the quads to be the same distance from the spacecraft X axis. Each quad is offset from the Y and Z axis and the jets are canted to reduce the thermal effects of the exhaust gas on the SM skin.

X component of RCS position	958.9	in.
Distance from jet to X axis	6.89	ft
Offset	7.25	deg
Cant	10	deg

6.10.2 Vehicle Mass Properties

Mass properties are presented for each of three different vehicle configurations: the CSM-only, the CSM docked with the full LM Ascent-Descent Configuration, and the CSM docked with the empty LM Ascent Stage.

The center of gravity and moments of inertial of the vehicle are computed as functions of total vehicle mass using a least-squares curve fit on 82 fuel data points to generate two sets of polynomial coefficients, one for the storage tank and one for the sump tank.

The polynomials fitted to the curves are of the form

$$P = \sum_{k=0}^n a_K M^K$$

where M is in slugs. The centers of gravity are measured in feet and the inertias in slugs ft².

The principal moments of inertia are defined as

$$I_{XX} = \int (Y^2 + Z^2) dm$$

$$I_{YY} = \int (X^2 + Z^2) dm$$

$$I_{ZZ} = \int (X^2 + Y^2) dm$$

and the products of inertia are defined as

$$J_{XY} = + \int XY \, dm$$

$$J_{XZ} = + \int XZ \, dm$$

$$J_{YZ} = + \int YZ \, dm$$

6.10.2.1 The Empty CSM Configuration

The Empty CSM includes the SLA ring and RCS propellant.

Mass	751.88	slugs	10.2
Curve-Fit Coefficients for the Sump Tank			10.3
	A_0	A_1	A_2
CG_X	$.974539438^2$	$-.288966331^{-1}$	$.112181054^{-4}$
CG_Y	$-.162673947^1$	$.239141573^{-2}$	$-.731027577^{-6}$
CG_Z	$.130175554^1$	$-.110282091^{-2}$	$.337119334^{-6}$
I_{XX}	$.164888331^4$	$.164654595^2$	-----
I_{YY}	$-.725881195^5$	$.217161712^3$	$-.860099539^{-1}$
I_{ZZ}	$-.861562667^5$	$.233884920^3$	$-.865211357^{-1}$
J_{XY}	$.143099699^5$	$-.256770983^2$	$.997922616^{-2}$
J_{XZ}	$-.699385787^4$	$.118178513^2$	$-.458638456^{-2}$
J_{YZ}	$-.125587571^4$	$.111737291^1$	$.299136797^{-3}$
Curve-Fit Coefficients for the Storage Tank			10.3
	A_0	A_1	A_2
CG_X	$.101623351^3$	$-.258668285^{-1}$	$.704619841^{-5}$
CG_Y	$.356847596^1$	$-.426294439^{-4}$	$.829889876^{-8}$
CG_Z	$-.485198234^1$	$.885097950^{-3}$	$-.184470384^{-6}$

	A_0	A_1	A_2
I_{XX}	.134156789 ⁴	.166489764 ²	-----
I_{YY}	-.176841735 ⁶	.267276695 ³	-.691784057 ⁻¹
I_{ZZ}	-.148224489 ⁶	.254455077 ³	-.694520184 ⁻¹
J_{YY}	-.300074061 ⁴	.104334938 ¹	-.281816724 ⁻³
J_{XZ}	.178006253 ⁵	-.197492239 ²	.540048995 ⁻²
J_{YZ}	-.584997323 ⁴	.479163704 ¹	.452222440 ⁻⁴

6.10.2.2 CSM and full LM Ascent-Descent Configuration

Mass	1766.80	slugs	10.2
Curve-Fit Coefficients for the Sump Tanks			10.3
	A_0	A_1	A_2
CG_X	.138925032 ³	-.381715205 ⁻¹	.726148855 ⁻⁵
CG_Y	-.171320337 ¹	.125734564 ⁻²	-.198606172 ⁻⁶
CG_Z	.603518093 ¹	-.228057558 ⁻³	.360231955 ⁻⁷
I_{XX}	.670742798 ⁴	.164143851 ²	-----
I_{YY}	-.175093183 ⁷	.176840413 ⁴	-.358483546 ¹
I_{ZZ}	-.178135365 ⁷	.178568870 ⁴	-.358836446 ¹
J_{XY}	.847425774 ⁵	-.701195962 ²	.133477225 ⁻¹
J_{XZ}	-.209560177 ⁵	.126892617 ²	-.241276177 ⁻²
J_{YZ}	-.309050458 ⁴	.167735629 ¹	.661247941 ⁻⁴

Curve-Fit Coefficients for the Storage Tank

10. 3

	A_0	A_1	A_2
CG_X	$.139697595^3$	$-.339248569^{-1}$	$.539720401^{-5}$
CG_Y	$-.109353660^{-2}$	$.105822398^{-3}$	$-.130583479^{-7}$
CG_Z	$-.102284910^1$	$.771202803^{-3}$	$-.10145265^{-6}$
I_{XX}	$.568595891^4$	$.168232359^2$	-----
I_{YY}	$-.224597471^7$	$.184509164^4$	$-.306987702^1$
I_{ZZ}	$-.220355725^7$	$.183248052^4$	$-.307226899^1$
J_{XY}	$.596858749^4$	$-.873825821^1$	$.139286026^{-2}$
J_{XZ}	$.830126612^5$	$-.587612974^2$	$.945108328^{-2}$
J_{YZ}	$-.107142372^5$	$.513303415^1$	$.788570758^{-4}$

6. 10. 2. 3 CSM and Empty LM Ascent Configuration

The empty LM ascent stage includes two crew members.

Mass 921.96 slugs 10. 2

Curve-Fit Coefficients for the Sump Tank

10. 3

	A_0	A_1	A_2
CG_X	$.10587677^3$	$-.32653398^{-1}$	$.10685749^{-4}$
CG_Y	$-.14871663^1$	$.19425638^{-2}$	$-.51311709^{-6}$
CG_Z	$.9913413^1$	$-.69759708^{-3}$	$.18337182^{-6}$
I_{XX}	$.212601452^4$	$.163318442^2$	-----
I_{YY}	$-.185665591^6$	$.413436025^3$	$-.141362881^1$
I_{ZZ}	$-.201408033^6$	$.430150299^3$	$-.141802258^1$
J_{XY}	$.224937387^5$	$-.321108387^2$	$.105186681^{-1}$
J_{XZ}	$-.994278483^4$	$.115090420^2$	$-.376489919^{-2}$
J_{YZ}	$-.220184720^4$	$.141074816^1$	$.180991649^{-3}$

Curve-Fit Coefficients for the Storage Tank

10.3

	A_0	A_1	A_2
CG_X	$.10852103^3$	$-.28094546^{-1}$	$.68026968^{-5}$
CG_Y	$.37312096$	$-.47401071^{-4}$	$.8389768^{-7}$
CG_Z	$-.68268762$	$.9148723^{-3}$	$-.17297510^{-5}$
I_{XX}	$.149142449^4$	$.167075445^2$	-----
I_{YY}	$-.337703110^6$	$.460629996^3$	$-.110802143^1$
I_{ZZ}	$-.306147195^6$	$.447738505^3$	$-.111047773^1$
J_{XY}	$-.356426251^4$	$.153248911^1$	$-.368334660^{-3}$
J_{XZ}	$.255052535^5$	$-.271964172^2$	$.661679522^{-2}$
J_{YZ}	$-.708545992^4$	$.479540000^1$	$.432501693^{-4}$

6.10.3 Service Module RCS Performance

6.10.3.1 The thrust from an RCS jet is displaced in time from the CMC on-off signal without thrust shaping. Propellant usage was treated as a constant-mass flow rate while the jet is firing, plus a dribble-volume penalty for each jet firing.

RCS thrust	100	lb	10.1
Propellant flow rate	0.001122	slugs/sec	10.1
Dribble penalty	0.00010256	slug	10.4
On delay	0.012	sec	10.4
Off delay	0.007	sec	10.4

6.10.4 Service Propulsion System

6.10.4.1 SPS Thrust and Time Delays

The SPS engine was modelled as a constant thrust, constant propellant flow rate motor. The build-up and tail-off of thrust are treated as instantaneous changes of force shifted in time from the electrical command.

Constant thrust	20,500	lb	10.8
Constant propellant flow rate	1.975	slugs/sec	10.5
SPS usable propellant	1165.5	slugs	10.3

On-Off delays

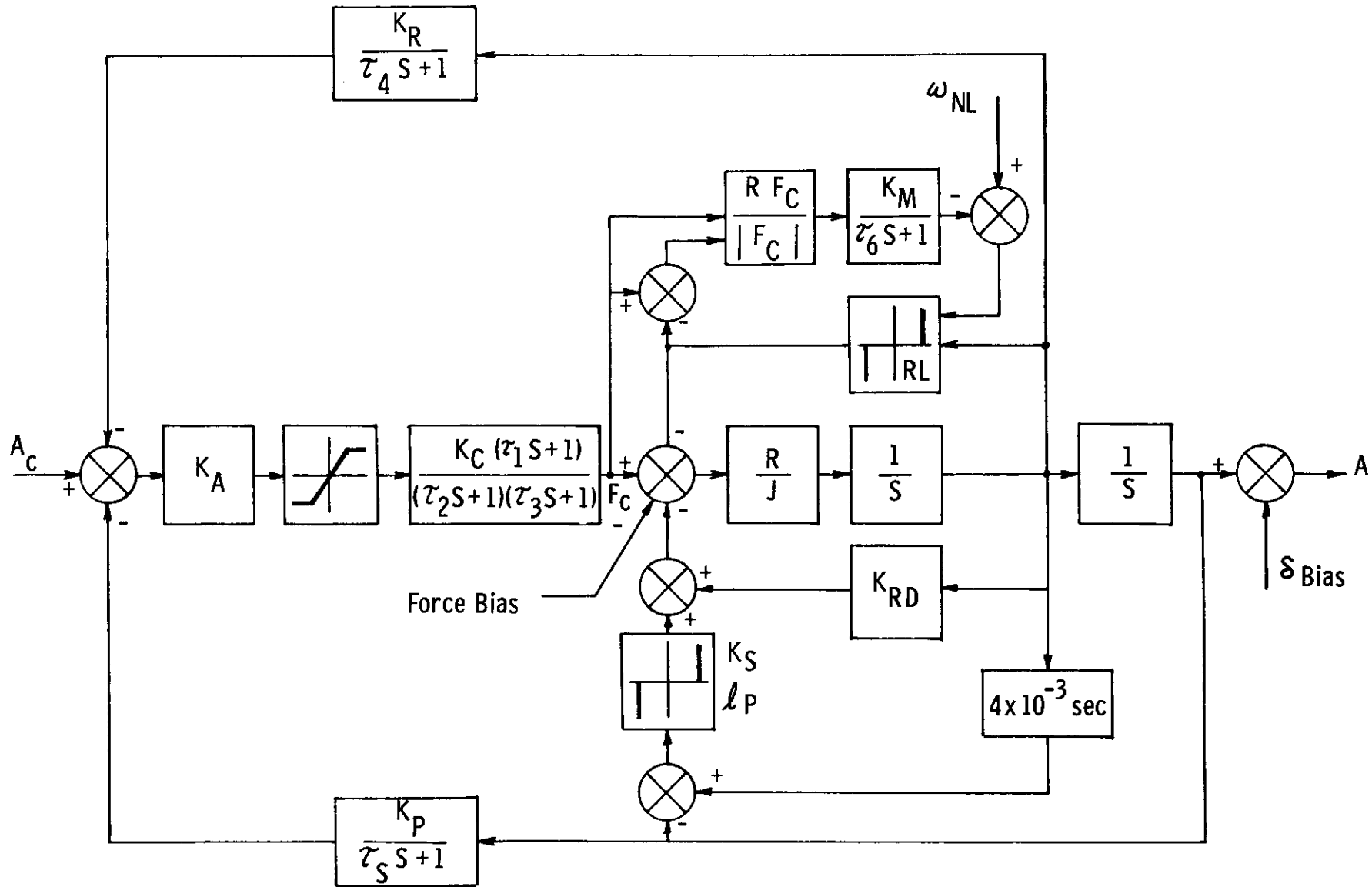
t is duration of electrical on command in seconds

$0 < t < 0.40$	no engine on	10.9
$0.40 < t < 1.00$	$\Delta t_{on} = 0.52$	10.9
	$\Delta t_{off} = 26.475 t_{on} - 6.590$	10.9
$1.00 < t$	$\Delta t_{on} = 0.52$	10.8
	$\Delta t_{off} = 0.49$	10.8

6.10.4.2 SPS Actuator Dynamics

The SPS engine angular position is controlled by closed-loop servomechanisms in pitch and yaw. All applicable dynamics have been included for the amplifier, clutch, motor, and feedback loops.

		Pitch	Yaw		
Amplifier gain	K_A	20	20	amps/rad	10.6
Current limit		$\pm .343$	$\pm .343$	amps	10.6
Clutch gain	K_C	3.5	3.5	lb/mA	10.6
time constant	τ_1	.0268	.0268	sec	10.6
time constant	τ_2	.0326	.0326	sec	10.6
time constant	τ_3	.0038	.0038	sec	10.6
Inertia	J	304	313	slugs/ft ²	10.6
Rate damping feedback gain	K_{RD}	1000	1000	lb sec	10.6



SPS Actuator Schematic

Snubber spring constant	K_S	6.72×10^6	7.02×10^6	lb/rad	10.6
Snubber spring position limit	ℓ_P	.0785	.0785	rad	10.6
Actuator lever arm	R	1	1	ft	10.6
Rate feedback gain	K_R	.0943	.0985	sec	10.6
time constant	τ_4	.00151	.00151	sec	10.6
Position feedback gain	K_P	1	1	nd	10.6
time constant	τ_5	.00794	.00794	sec	10.6
Null bias	δ_{bias}	-2.15	0.95	deg	10.1
Motor lag-time constant	τ_6	.1	.1	sec	
Motor gain	K_M	1.02×10^{-4}	1.02×10^{-4}	$\frac{\text{rad/sec}}{\text{ft lb}}$	
Motor no-load speed	ω_{NL}	.212	.206	rad/sec	
Motor rate limit constant	RL	1.68×10^6	1.754×10^6	lb/rad/sec	

6.10.5 Spacecraft Bending with LM attached

With the LM attached, the combined vehicle will have 3 degrees of bending. Bending parameters were determined to have a constant value equal to the average between the full and half-full vehicle; this represents the range of values expected for Mission D.

Values given are the X, Y, Z components of the indicated mode at a particular station. Because of the coupling of the Modes, the damping ratios were made the same.

$$\omega_1 = 13.5 \text{ rad/sec}$$

$$\xi = .005$$

ϕ_1 (XA)	-.058	-.0234	-.020	nd
ϕ_1 (XB)	.018	-.017	-.029	nd
ϕ_1 (XC)	.050	-.007	-.022	nd
ϕ_1 (XD)	-.025	-.013	-.013	nd

$$\omega_2 = 14.4 \text{ rad/sec}$$

$$\xi = .005$$

ϕ_2 (XA)	.027	-.043	.021	nd
ϕ_2 (XB)	.049	-.026	-.004	nd
ϕ_2 (XC)	-.028	-.002	.014	nd
ϕ_2 (XD)	-.051	-.017	.039	nd

$$\omega_3 = 15.4 \text{ rad/sec}$$

$$\xi = .005$$

ϕ_3 (XA)	.007	.061	-.015	nd
ϕ_3 (XB)	.021	.010	.059	nd
ϕ_3 (XC)	-.008	.070	.053	nd
ϕ_3 (XD)	-.021	-.019	-.067	nd

ϕ_1 (XT)	-.0034	.042	.064	nd
ϕ_2 (XT)	-.00060	.053	-.040	nd
ϕ_3 (XT)	-.0025	.028	-.023	nd

σ_1 (XT)	----	.00792	-.00552	rad/ft
σ_2 (XT)	----	-.00516	-.00720	rad/ft
σ_3 (XT)	----	-.00180	-.00264	rad/ft

ϕ_1 (X _{NB})	----	-.059	-.087	nd
ϕ_2 (X _{NB})	----	-.081	.063	nd
ϕ_3 (X _{NB})	----	.028	.0085	nd

σ_1 (X _{NB})	.00018	.00720	-.00432	rad/ft
σ_2 (X _{NB})	.000528	-.00468	-.00540	rad/ft
σ_3 (X _{NB})	.00144	-.00120	-.00276	rad/ft

6.10.6 Propellant Slosh

Slosh motion of the propellant in the SPS tanks is simulated during SPS thrusting as a linear spring mass system that can be characterized by a sloshing mass (constant for each tank), a slosh frequency (a function of mass for each tank), and an attachment point (a function of propellant mass). Sloshing can occur in the two storage tanks (full sump tanks) or in the two sump tanks (empty storage tanks).

In addition, when the LM is attached, the LM propellant will slosh when the SPS engine is on. The LM slosh parameters are held fixed.

6.10.6.1 CSM Slosh Data

10.1

The total vehicle mass in slugs is represented by M.

		Storage	Sump	
Slosh frequency squared		21500/M	19000/M	rad ² /slugs ²
Oxidizer slosh mass		24.0	35.0	slugs
Fuel slosh mass		15.0	22.0	slugs
Fuel tank	Y coordinate	-1.233	-4.025	ft
Fuel tank	Z coordinate	-3.983	-0.55	ft
Oxidizer tank	Y coordinate	1.233	4.025	ft
Oxidizer tank	Z coordinate	3.983	0.55	ft
Fuel spring constant		323000/M	418000/M	lb/ft
Oxidizer spring constant		516000/M	665000/M	lb/ft
Damping ratio		0.0007	0.0007	nd

6.10.6.2 LM Slosh Data

10.7

Slosh frequency		3.7	rad/sec
Damping ratio		0.005	nd
Fuel slosh mass		11.4	slugs

Oxidizer slosh mass	19.0	slugs
Fuel spring constant	156.0	lb/ft
Oxidizer spring constant	260.0	lb/ft
Slosh moment arm	13.0	ft

6.11 Hybrid Simulator CM Spacecraft Data

6.11.1 CM Mass Properties

11.1

The mass properties are assumed to be constant at their values after separation prior to reentry and mass is not decremented due to RCS fuel usage or ablative heat shield loss.

Mass		409.12	slugs
Center of Gravity	X_{CG}	1045.1	in.
	Y_{CG}	-0.4	in.
	Z_{CG}	6.0	in.
Inertia	I_{XX}	6427	slug ft ²
	I_{YY}	5866	slug ft ²
	I_{ZZ}	5149	slug ft ²
	J_{XY}	59.5	slug ft ²
	J_{XZ}	-461.1	slug ft ²
	J_{YZ}	21.7	slug ft ²

6.11.2 CM RCS Data

11.2

The thrust from a RCS jet is displaced in time from the AGC on-off command without thrust shaping or atmospheric effects. The acceleration of the spacecraft due to jet firing is neglected.

Thrust	93.6	lb
Propellant flow rate	0.001122	slug/sec
Dribble penalty	0.00010256	slug

The X, Y, and Z components of the moment arm of each jet are given in feet.

Jet	X	Y	Z
1	-.27161	4.77114	.35428
2	.36075	-3.33500	0
3	0	5.75962	-.30553
4	-.29408	-3.33500	0

Jet	X	Y	Z
5	-. 33897	. 69558	5. 41832
6	. 34175	. 69558	-5. 36956
7	-. 34175	0	5. 41832
8	. 33898	0	-5. 36956
9	5. 14500	1. 04895	-. 19362
10	-5. 07944	1. 04895	. 19362
11	4. 51783	0	-1. 06579
12	-4. 86809	0	1. 06579

6. 11. 3 CM Entry Aerodynamics

11. 2

The aerodynamic forces and moments acting on the spacecraft during reentry are calculated from three aerodynamic coefficients: $C_A(\alpha, M)$, the axial-force coefficient; $C_N(\alpha, M)$, the normal-force coefficient; and $C_M(\alpha, M)$, the pitching-moment coefficient about the theoretical CM cone apex. These are computed using a linear bivariate interpolation scheme as a function of angle of attack α and Mach number M .

Moment reference center	1141. 25	in.
	0. 0	in.
	0. 0	in.
Reference area	129. 35	ft ²
Reference length	154. 0	in.

CA

M \ α	145.1365	150.1365	155.1365	160.1365	165.1365	170.1365	175.1365	180.1365
.7	-.9100	-.9501	-.9801	-1.0001	-1.0220	-1.0199	-1.0099	-0.9800
.9	-.9902	-1.0452	-1.0751	-1.1051	-1.1200	-1.1150	-1.1010	-1.0900
1.1	-1.2102	-1.2402	-1.2701	-1.2901	-1.3051	-1.3150	-1.3150	-1.3050
1.2	-1.2072	-1.2302	-1.2501	-1.2801	-1.3001	-1.3100	-1.3200	-1.3250
1.35	-1.3103	-1.3702	-1.4001	-1.4051	-1.4101	-1.4150	-1.4200	-1.4200
1.65	-1.2703	-1.3502	-1.3902	-1.4201	-1.4301	-1.4400	-1.4420	-1.4580
2.0	-1.2294	-1.3253	-1.4022	-1.4361	-1.4530	-1.4670	-1.4710	-1.4720
2.4	-1.1904	-1.2803	-1.3582	-1.4051	-1.4401	-1.4550	-1.4650	-1.4700
3.0	-1.1404	-1.2303	-1.3202	-1.3802	-1.4201	-1.4501	-1.4700	-1.4750
4.0	-1.0924	-1.1903	-1.2752	-1.3412	-1.3961	-1.4341	-1.4540	-1.4600
6.0+	-1.0828	-1.1763	-1.2672	-1.3452	-1.4138	-1.4611	-1.4840	-1.4900

		CN							
M \ α		145.1365	150.1365	155.1365	160.1365	165.1365	170.1365	175.1365	180.1365
.7		.0178	.0227	.0327	.0276	.0076	-.0224	-.0274	-.0023
.9		.0756	.0675	.0524	.0354	.0173	-.0027	-.0126	-.0026
1.1		.0871	.0650	.0490	.0349	.0219	.0019	-.0131	-.0031
1.2		.0871	.0621	.0520	.0370	.0219	.0069	-.0011	-.0032
1.35		.1319	.0717	.0517	.0367	.0216	.0096	.0066	-.0034
1.65		.1440	.1018	.0667	.0416	.0246	.0126	.0026	-.0035
2.0		.1591	.1218	.0847	.0466	.0185	.0065	-.0015	-.0035
2.4		.1592	.1220	.0868	.0587	.0366	.0185	.0065	-.0035
3.0		.1573	.1221	.0949	.0697	.0476	.0315	.0145	-.0035
4.0		.1464	.1202	.0930	.0693	.0479	.0291	.0116	-.0035
6.0+		.1424	.1202	.0960	.0748	.0526	.0305	.0115	-.0035

CM

M \ α	145.1365	150.1365	155.1365	160.1365	165.1365	170.1365	175.1365	180.1365
.7	.0834	.0603	.0385	.0304	.0333	.0419	.0327	.0038
.9	.0245	.0210	.0212	.0233	.0246	.0271	.0171	.0042
1.1	.0160	.0161	.0170	.0189	.0178	.0212	.0155	.0050
1.2	.0149	.0185	.0147	.0164	.0175	.0184	.0154	.0051
1.35	-.0177	.0149	.0181	.0177	.0184	.0170	.0094	.0054
1.65	-.0294	-.0075	.0061	.0132	.0146	.0135	.0110	.0056
2.0	-.0424	-.0223	-.0050	.0108	.0197	.0188	.0135	.0057
2.4	-.0433	-.0237	-.0067	.0026	.0079	.0088	.0072	.0057
3.0	-.0416	-.0243	-.0126	-.0036	.0006	.0010	.0025	.0057
4.0	-.0319	-0.209	-.0090	.0023	.0013	.0037	.0033	.0057
6.0+	-.0194	-.0103	-.0016	.0033	.0003	.0114	.0129	.0137

6.12 Hybrid Simulation Coordinate Systems and Natural Environment Data

6.12.1 Reference Coordinate System

The reference inertial coordinate system is defined in Section 6.7.

All spacecraft state vectors and attitudes are referenced to this coordinate system.

6.12.2 Earth Gravitation Model

12.1

Accelerations due to the gravitational attraction of the earth were computed from

$$\underline{a}_E = \frac{\mu_E}{r^2} \sum_{i=2}^4 J_{iE} \left(\frac{r_E}{r}\right)^i \left[P'_{i+1}(\cos \phi) \underline{u}_R - P'_i(\cos \phi) \underline{u}_Z \right]$$

where

$$r_E = 6378165 \text{ m} \quad \text{equatorial radius of the earth}$$

$$\mu_E = 0.3986032 \times 10^5 \text{ M}^3/\text{S}^2 \quad \text{gravitational parameter}$$

$$J_{2E} = 0.10823 \times 10^{-2} \quad \text{oblateness coefficients}$$

$$J_{3E} = -0.23 \times 10^{-5}$$

$$J_{4E} = -0.18 \times 10^{-5}$$

r is length of position vector

\underline{u}_R is the unit position vector

\underline{u}_Z is unit vector along the polar axis

$$P'_2(\cos \phi) = 3 \cos \phi$$

$$P'_3(\cos \phi) = 1/2 (15 \cos^2 \phi - 3)$$

$$P'_4(\cos \phi) = 1/3 (7 \cos \phi P'_3 - 4 P'_2)$$

$$P'_5(\cos \phi) = 1/4 (9 \cos \phi P'_4 - 5 P'_3)$$

$$\cos \phi = \underline{u}_R \bullet \underline{u}_Z$$

6.12.3 Moon Gravitation Model

When the moon is the primary body, no influence of a secondary body is considered. The gravitational accelerations due to the primary body are computed from:

$$\underline{a}_M = \frac{\mu_M}{r^2} \left\{ J_{2M} \left(\frac{r_M}{r} \right)^2 \left[P_3'(\cos \phi) \underline{u}_r - P_2'(\cos \phi) \underline{u}_z \right] \right. \\ \left. + 3 J_{22M} \left(\frac{r_M}{r} \right)^2 \left[4 \frac{X_M Y_M}{X_M^2 + Y_M^2} (\underline{u}_r \times \underline{u}_z) \right. \right. \\ \left. \left. + \frac{X_M^2 - Y_M^2}{X_M^2 + Y_M^2} \left((5 \cos^2 \phi - 3) \underline{u}_r - 2 \cos \phi \underline{u}_z \right) \right] \right\}$$

where

$$r_M = 1738090 \text{ m} \quad \text{equatorial radius of the moon}$$

$$\mu_M = 0.4902778 \times 10^{13} \text{ M}^3/\text{S}^2 \quad \text{gravitational parameter}$$

$$J_{2M} = 0.207108 \times 10^{-3} \quad \text{oblateness coefficient}$$

$$J_{22M} = 0.207160 \times 10^{-4}$$

r is length of position vector $\{X_M, Y_M, Z_M\}$

$\underline{u}_r, \underline{u}_z, P_i', \cos \phi$ defined analogous to the earth.

6.12.4 Atmospheric Model

The atmospheric model is the 1962 U. S. Standard atmosphere; atmospheric perturbations due to winds are not included in the model. The model is described in Section 6.7.

When the LM is present and within 327 miles of the CSM, range data is transmitted from a VHF simulator to the CMC.

The simulator is a 15-bit shift register, preset during the simulator state-vector update calculation once-a-second, asynchronous to the CMC.

Each bit represents 0.01 mile.

6.14 References

- 2.1 Directory of Standard Geodetic and Geophysical Constants for Gemini and Apollo, NASA General Working Paper, No. 10, 020B, 6 April 1966.
- 2.2 Natural Environment and Physical Standards for the Apollo Program, NASA, M-D E 8020.008B, SE 015-001-1, April 1965.
- 2.3 CSM/LM Spacecraft Operational Data Book, Vol. I, CSM Data Book, Manned Spacecraft Center, SNA-8-D-027, May 1968
- 2.4 Undocumented Estimate.
- 2.5 MIT Apollo Guidance and Navigation Information Massachusetts Institute of Technology, Instrumentation Laboratory, G-532, 28 November 1962.
- 3.1 Saturn V AS-504 Launch Vehicle Guidance and Navigation Error Analysis, The Boeing Company, D5-15708-4, 27 November 1967.
- 3.2 Saturn V AS-504 Launch Vehicle Guidance and Navigation Error Analysis, NASA George C. Marshall Spaceflight Center, R-AERO-DGA-1-68, 13 February 1968.
- 3.3 Saturn V AS-504 Launch Vehicle Reference Trajectory, The Boeing Company, D5-15481-1, 15 May 1967.
- 3.4 Control System Math Models for Switchover Studies, NASA George C. Marshall Spaceflight Center, R-ASTR-F-66-56, 1 April 1966.
- 3.5 Saturn V Launch Vehicle Guidance Equations, SA504, The Boeing Company, D5-15706-4, 15 July 1967.
- 4.1 Block II, G&N Navigational Base and Optics Assembly to Command Module Structure, MIT and North American Aviation, Inc., Interface Control Document MH01-01301-116, 1 June 1967.
- 4.2 CSM/LM Spacecraft Operational Data Book, Volume I, CSM Data Book, NASA, SNA-8-D-027, May 1968.

- 4.3 CSM/LM Spacecraft Operation Data Book, Volume III, Mass Properties, NASA, SNA-8-D-027, Amendment 2, 20 May 1968.
- 4.4 CSM-103 Apollo Technical Information Listing, NASA, 68-FS55-3-20, 19 January 1968.
- 4.5 Apollo Mission Data Specification C-Apollo Saturn 207/208A, TRW Systems, 2131-H005-R8-000, 9 June 1966.
- 4.6 Performance Data Supplement to Mission Modular Data Book-Block II Earth Orbital Mission, North American Aviation, Inc., SID 66-1501-A, Revised 15 March 1967.
- 4.7 LM-3 Mass Properties Data, US Memorandum, PM3/M-215/67, 6 October 1967.
- 4.8 A Comparison Between a "Static" and "Dynamic" Liquid Propellant Method for Calculating LM Mass Properties, Grumman Aircraft Engineering Corporation, LMO 500-583, 1 June 1967.
- 4.9 Conversations with NAR Propulsion Groups, 23 May 1968.
- 4.10 Three Dimensional Vibrational Modes of the Apollo CSM/LM Docked Vehicles, TRW Systems Report No. 05952-H300-R000, 29 September 1967.
- 4.11 Three Dimensional Vibrational Modes of the Apollo CSM/LM Docked Vehicles, TRW Systems Report No. 05952-H342-R000, 20 November 1967.
- 4.12 Three Dimensional Vibrational Modes of the Apollo CSM/LM Docked Vehicles, TRW Systems Report No. 05952-H239-R000, 30 June 1967.
- 5.1 Block II, G&N Navigational Base and Optics Assembly to Command Module Structure, MIT and North American Aviation, Inc., Interface Control Document MH01-01301-116, 1 June 1967.
- 5.2 Performance Data Supplement to Mission Modular Data Book - Block II Earth Orbital Mission, North American Aviation, Inc., SID 66-1501-A, Revised 15 March 1967.

- 5.3 CSM/LM Spacecraft Operational Data Book, Volume I, CSM Data Book, NASA, SNA-8D-027, May 1968.
- 6.1 Apollo VHF Ranging Preliminary Design Review, North American Aviation, Inc., MS-901-0712D, 19 December 1967.
- 6.2 Command Module Guidance Computer Electrical Interfaces, Block II, NAA-MIT, North American Aviation, Inc., MH01-01380-216, 15 December 1967.
- 7.1 Directory of Standard Geodetic and Geophysical Constants for Gemini and Apollo, NASA General Working Paper No. 10,020B, 6 April 1966.
- 7.2 U. S. Standard Atmosphere, 1962, published under the sponsorship of NASA, U. S. Air Force, and U. S. Weather Bureau, December 1962.
- 10.1 CSM/LM Spacecraft Operational Data Book, Volume I, (SNA-8-D-027), MSC, May 1968.
- 10.2 CM 103, LM3 Mass Properties, MSC-S-59, 14 November 1967.
- 10.3 TRW AMDS, 2131-H002-T8-000.
- 10.4 Coordination with MSC-SSM on 20 November 1967, (R. Taeuber - MSC and J. Owen/G. Holland - TR - TRW).
- 10.5 Performance Data Supplement, NAA SID 66-1501-A, Revision, 15 March 1967.
- 10.6 Internal Letter, North American Aviation, 190-600-BII-67-018, 9 August 1967.
- 10.7 LM GN&C Data Book: GAEC-S-7, 13 October 1965.
- 10.8 Undocumented Data from North American Aviation Propulsion Group, 23 May 1968.
- 10.9 Memorandum from FM7/Guidance and Performance Branch/Guidance Analysis Section/MS, 68-FM7 3-239, 22 May 1968.

- 11.1 Preliminary CSM 103 and LM3 Mass Properties Summary,
14 November 1967.
- 11.2 CSM/LM Spacecraft Operational Data Book, Volume I, SNA-8-D-027,
MSC, May 1968.
- 12.1 Natural Environment and Physical Standards for the Apollo Program,
NASA, M-DE-8020-008B, April 1965.
- 13.1 Command Module Guidance Computer Electrical Interfaces, Block II,
NAA-MIT, North American Aviation, Inc., MH01-01380-216,
15 December 1967.

COLOSSUS
Section 4 (Rev 6)

Internal:

Adler, P.	Grace, E.	Levine, G.	Schlundt, R.
Bairnsfather, R.	Greene, K.	Lickly, D. (3)	Schmidt, W.
Battin, R.	Griggs, K.	Lones, R.	Scholten, R.
Beals, C.	Hamilton, M.	Marscher, W.	Schroeder, S.
Blanchard, E.	Haslam, R.	Martin, F.	Schulenberg, C.
Cooper, W.	Heinemann, P.	McOuat, H.	Schulte, R.
Copps, E.	Henize, J.	Megna, V.	Sears, N.
Copps, S.	Hoag, D.	Metzinger, R.	Sewall, A.
Cox, G.	Hsiung, D.	Millard, D.	Shillingford, J.
Davis, S.	Hughes, E.	Miller, J.E.	Sokkappa, B.
Day, W.	Ireland, B.	Miller, J.S.	Sprague, D.
DeCain, F.	Issacs, T.	Mimno, P.	Stameris, W.
Denniston, E.	Johnson, I.	Morse, J. (10)	Stubbs, G.
Deutsch, S.	Johnson, L. B.	Morth, R.	Suomala, J.
DeWolf, D.	Johnson, M.	Muller, E.	Sutherland, J.
Dimock, G.	Johnston, M.	Nevins, J.	Tanner, W.
Drake, L.	Keene, D.	O'Connor, J.	Tinkham, R.
Drane, L.	Kernan, J.	Ostaneck, W.	Turnbull, J.
Dunbar, J.	Kiburz, R.	Parr, T.	Vincent, K.
Dunbar, V.	Kido, K.	Philliou, P.	Vitteck, J.
Edmonds, G.	*Kingston, J.	Plender, P. (6)	Volante, P.
Eliassen, S.	Klumpp, A.	Pope, G.	Weatherbee, R.
Engel, A. (2)	Kosmala, A.	Pu, C.	Wenk, C.
Felleman, P.	Kossuth, G.	Ragan, R.	Werner, R.
Fleming, J.	Kupfer, W.	Riebesell, K.	White, P.
Gediman, L. (20)	Laats, A.	Robertson, W.	White, R.
Glendenning, J.	Larson, L.	Rye, P. (3)	Widnall, W.
Glick, K.	Larson, R.	Sapanaro, J. (4)	Wolff, P.
Goldberger, S.	Lawrence, J.	Sarda, P.	Womble, M.
Goodwin, K.	Leone, F.	Savatsky, S.	Zeldin, S.
			Apollo Library (2)
			MIT/IL Library (6)

*Letter of transmittal only.

MIT Instrumentation Laboratory (1)
c/o North American Rockwell, Inc.
Space and Information Division
12214 Lakewood Boulevard
Downey, California 90241
Attn: Mr. Thomas A. Hemker

MIT Instrumentation Laboratory
G&N Systems Laboratory (1)
c/o Grumman Aircraft Engineering Corp.
LM Project - Plant 25
Bethpage, Long Island, New York
Attn: Mr. James A. Hand

MIT Instrumentation Laboratory (5)
P. O. Box 21025
Kennedy Space Center, Florida 32815
Attn: Mr. George Silver

MIT Instrumentation Laboratory (3)
Code EG/MIT Building 16
NASA Manned Spacecraft Center
Houston, Texas 77058
Attn: Mr. Thomas Lawton (10)

NASA MSC HW
Building M7-409
Kennedy Space Center, Florida 32815
Attn: Mr. Frank Hughes

Mr. A. Metzger (NASA/RASPO at MIT/IL) (1)

AC Electronics Division (15)
General Motors Corporation
Milwaukee, Wisconsin
Attn: Mr. J. Stridde Dept. 32-31 (13)
Attn: Mr. Reino Karell (2)

Kollsman Instrument Corporation (1)
575 Underhill Boulevard
Syosset, Long Island
Attn: Mr. F. McCoy

Raytheon Company (6)
Boston Post Road
Sudbury, Massachusetts 01776
Attn: Mr. J. Shrmack

NASA/RASPO/National Aeronautics and Space Administration (1)
NAR Resident Apollo Spacecraft Program Office
North American Rockwell, Inc.
Space and Information Systems Division
12214 Lakewood Boulevard
Downey, California

NASA/KSC (3)
National Aeronautics and Space Administration
John F. Kennedy Space Center
J. F. Kennedy Space Center, Florida 32899
Attn: Technical Document Control Office

NASA/RASPO GE	NASA Daytona Beach Operation P.O. Box 2500 Daytona Beach, Florida 32015 Attn: Mr. A. S. Lyman	(1)
NASA/HDQ	NASA Headquarters 600 Independence Avenue SW Washington, D.C. 20546 Attn: MAP-2 Attn: Mission Director, Code MA Attn: Robert Aller, Code MAO	(6) (4) (1) (1)
NASA/LEWIS	National Aeronautics and Space Administration Lewis Research Center Cleveland, Ohio Attn: Library	(2)
NASA/FRC	National Aeronautics and Space Administration Flight Research Center Edwards AFB, California Attn: Research Library	(1)
NASA/LRC	National Aeronautics and Space Administration Langley Research Center Langley AFB, Virginia Attn: Mr. A. T. Mattson	(2)
NASA/GSFC	National Aeronautics and Space Administration Goddard Space Flight Center Greenbelt, Maryland Attn: Mr. Paul Pashby, Code 813	(2)
GAEC	Grumman Aircraft Engineering Corporation Bethpage, Long Island, New York Attn: Mr. J. Marino Mr. R. Pratt	(2) (1) (1)
NAR	North American Rockwell Inc. Space and Information Systems Division 12214 Lakewood Boulevard Downey, California 90241 Attn: Apollo Data Requirements Dept. 096-340 Building 3, CA 99	(1 + 1R)

NASA/RASPO GAEC	National Aeronautics and Space Administration Resident Apollo Spacecraft Program Officer Grumman Aircraft Engineering Corporation Bethpage, Long Island, New York	(1)
NASA/RASPO ACED	National Aeronautics and Space Administration Resident Apollo Spacecraft Program Officer AC Electronics Division General Motors Corporation Milwaukee, Wisconsin 53201 Attn: Mr. W. Swingle	(1)
NASA/WSMR:	National Aeronautics and Space Administration Post Office Drawer MM Las Cruces, New Mexico Attn: RH4 Documentation	(2)
NASA/MSFC:	National Aeronautics and Space Administration George C. Marshall Space Flight Center Huntsville, Alabama Attn: J. Mack R-ASTR-5 (1) H. Ledford R-AERO-P (2) L. McNair R-AERO-P (1) E. Deaton R-AERO-DA (1) A. Deaton R-AERO-DG (1) L. Stone R-AERO-F (1) C. Hagood R-AERO-F (1) O. Hardage R-AERO-FM (1) F. Moore R-ASTR-N (1) S. Seltzer R-ASTR-NG (5) H. Hosenthien R-ASTR-F (1) A. McNair I-MO-R (1) D. Germany I-I/IB-E (1) R. Barraza I-V-E (1) W. Chubb R-ASTR/NG (1) J. McCullough I-VE/T (1)	(21)
NASA/MSC	National Aeronautics and Space Administration Manned Spacecraft Center Apollo Document Control Group (PA 2) Houston, Texas 77058 Attn: A. Alber, FS5 (letter of transmittal only)	300 + 2R
BELLCOMM:	Bellcomm, Inc. 1100 17th Street N.W. Washington, D.C. 20036 Attn: Info. Analysis Section	(6)
LINK:	LINK Group, GPSI SIMCOM 1740 A NASA Boulevard Houston, Texas 77058 Attn: Mr. D. Klingbell	(3)
TRW:	Gilbert H. Friedman Building 82 Rm 2067 TRW System Group One Space Park Redondo Beach, California 90278	(5)